

**Tailored Design of Boron-Doped Diamond Electrodes
for Electrochemical Reduction of CO₂**

July 2020

XU, Jing

A Thesis for the Degree of Ph.D. in Engineering

**Tailored Design of Boron-Doped Diamond Electrodes
for Electrochemical Reduction of CO₂**

July 2020

Graduate School of Science and Technology

Keio University

XU, Jing

Table of Content

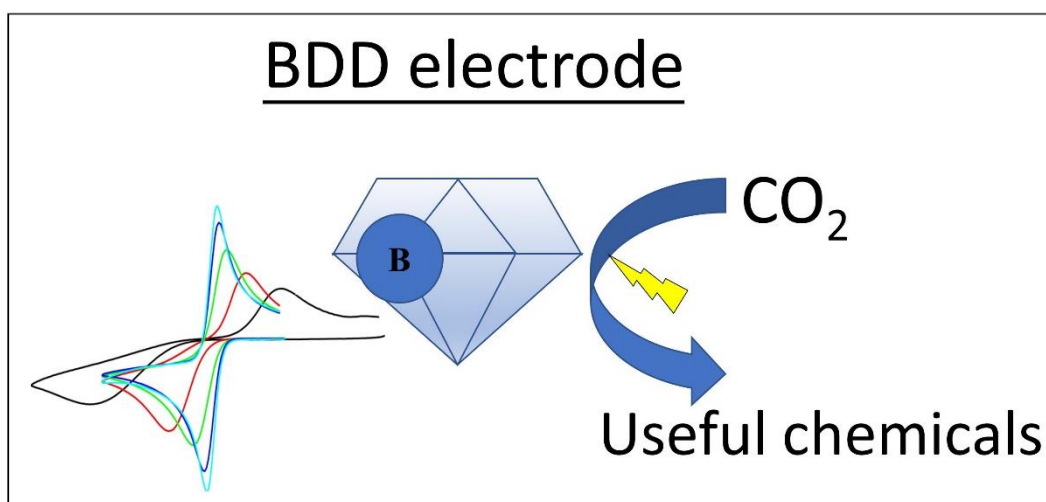
Chapter 1 General introduction	1
1.1 Conversion of green-house gas CO ₂	2
1.1.1 Motivation of converting CO ₂	2
1.1.2 Artificial CO ₂ conversion.....	3
1.2 Boron doped diamond.....	9
1.2.1 Composition of boron-doped diamond.....	9
1.2.2 Electrochemistry properties of BDD.....	12
1.2.3 Applications of BDD electrode.....	13
1.3 Electrochemical reduction of CO ₂ on BDD electrode.....	14
1.4 Outline of this thesis.....	15
1.5 References.....	16
Chapter 2 Effect of boron doping level on the electrochemical reduction of CO₂ on boron doped diamond electrodes	25
2.1 Introduction.....	26
2.2 Experimental.....	26
2.3 Results and discussion.....	28
2.3.1 Structural characterization of BDD electrodes.....	28
2.3.2 Electrochemical properties of BDD electrodes.....	31
2.3.3 Performance of BDD electrodes for the electrochemical reduction of CO ₂	33
2.3.4 Possible mechanism for CO ₂ reduction on BDD electrodes with various boron contents.....	35

2.4 Conclusion	37
2.5 References.....	37
Chapter 3 Unusual electrochemical properties of low-doped boron-doped diamond electrodes containing sp² carbon	40
3.1 Introduction	41
3.2 Experimental	42
3.2.1 Sample Preparation.....	42
3.2.2 Characterization.....	43
3.2.3 Electrochemical Measurement.....	45
3.2.4 XPS/UPS Measurement	46
3.3 Results and discussion.....	47
3.3.1 Characteristics.....	47
3.3.2 Electrochemical Properties	50
3.3.3 Surface Analysis	55
3.4 Conclusion	61
3.5 References.....	61
Chapter 4 Effect of sp² species in a boron-doped diamond electrode on the electrochemical reduction of CO₂	68
4.1 Introduction	69
4.2 Experimental	69
4.2.1 Preparation of BDD working electrode	69
4.2.2 Electrochemical reduction of CO ₂	70
4.3 Results and discussion.....	72
4.3.1 Characterization of the BDDs.....	72

4.3.2 CO ₂ reduction on sp ² -containing BDD	72
4.3.3 Mechanism proposal.....	77
4.4 Conclusion	78
4.5 References.....	79
Chapter 5 Summary and Future Perspective.....	82
5.1 Summary	83
5.2 Future perspective	84
List of Publications and Conferences	87
Curriculum Vitae.....	89
Acknowledgment	89

Chapter 1

General Introduction



1.1 Conversion of green-house gas CO₂

1.1.1 Motivation of converting CO₂

As human activities of combustion of fossil fuel and deforestation increase, significant upward rise of atmospheric CO₂, severe environment and energy problems have occurred. According to the data from National Oceanic and Atmospheric Administration (NOAA) of U.S., the concentration of green-house gas CO₂ in April 2020 (412 parts per million (ppm) [1]) hit a historical high record (Fig. 1.1). Ozone hole and global warming are the most well-known impacts of green-house effect. Furthermore, severe nature disaster, like unprecedented size wildfires in Australia and desert locust outbreak in Africa in 2019, are related with those climate changes as well [2]. The environmental crisis due to greenhouse gas emissions is motivating researchers to capture and convert CO₂.

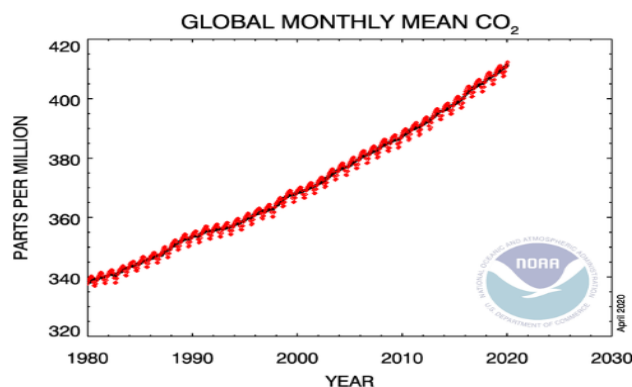
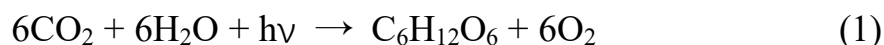


Fig. 1.1 Globally concentration (in ppm) [2].

In nature, CO₂ serves as carbon source of photosynthesis of plants and other organisms [3]. It is indicated in Eqn. (1) that, CO₂ and water are converted the into glucose and O₂ through plants using the energy from light (hν). Furthermore, CO₂ conversion was supposed existing even on Mars [4]. In this system, galvanic cell provides electronic energy and ferrous ions in magnetite serves as catalyst that would facilitate the reduction of CO₂. These

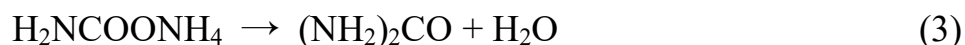
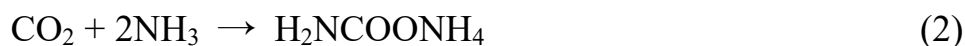
natural reactions inspired humans to convert CO₂ into useful chemicals and fuels as a novel strategy for environmental and energy problems [5–8].



1.1.2 Artificial CO₂ conversion

CO₂ conversion in industry

In chemical industry, CO₂ was extensively utilized as a viable feedstock for producing, e.g. urea, methanol, salicylic acid, formaldehyde [7]. The industrial reaction that consumes most CO₂ as reagent is Bosch-Meiser process, which was first developed in 1922 [9]. This is a standard way of producing urea until now, with CO₂ and ammonia as reagent under high temperature and pressure (eqn. (2) and (3)). On the other hand, CO₂ is also playing an important role of industrial producing methanol. In the process of methanol production, Cu-based ZnO/Al₂O₃ is used as catalyst and synthesis gas (CO, CO₂, H₂) is the reactant. This process is operated at pressure less than 100 bar and temperature around 490-570 K [10] (eqn. (4), (5) and (6)). Industrial conversion of CO₂ is achieved based on above reactions, but either with high pressure, high temperature or exothermal, which are not easy to control.



CO₂ conversion in lab

(1) Biological process

CO₂ conversions using biological processes in laboratories with mild environment were extensively investigated, which is rather different from the critical process in chemical industry. Enlightened by natural photosynthesis, some organisms like cyanobacteria [11], acetogens [12], *E. coli* [13] are used for CO₂ conversion. It takes the advantage of low-cost, since many organisms can be cultivated with cheap and ubiquitous gaseous carbon feedstocks. Even industrial waste gas, biogas and syngas can be used as gaseous carbon feedstock, because they are composed by CO₂, CO and hydrogen. However, maintaining the activity of organism during/after CO₂ conversion remained as a crucial problem.

(2) Photocatalysis conversion of CO₂

Photocatalytic method for CO₂ conversion is a hot topic in recent decades, since it could utilize light energy as shown in Fig. 1.2(a) [14–18]. In certain systems of photocatalysis, light energy can be utilized to allow the proceeding of CO₂ reduction at applied electric potentials more positive than the formal redox potential.

Semiconductors are by far the most commonly studied photocatalyst, since they would take advantage of their photogenerated current/voltage and perform good catalytic activity. An ideal semiconductor-based photocatalyst should possess appropriate band structure [17]: (1) medium band gap (1.7~3.1 eV) that can utilize the visible light efficiently and (2) appropriate location of the conduction band and valence band that deliver adequate redox potentials for CO₂ reduction. Semiconductor materials (as in Fig. 1.2(b)) including metal oxides (TiO₂, ZnO, WO₃ etc.) [19,20], layered double hydroxides [21] and metal chalcogenides (CdS, ZnS etc) [16,22] have been employed for CO₂ photocatalysis reaction and showed relatively good selectivity.

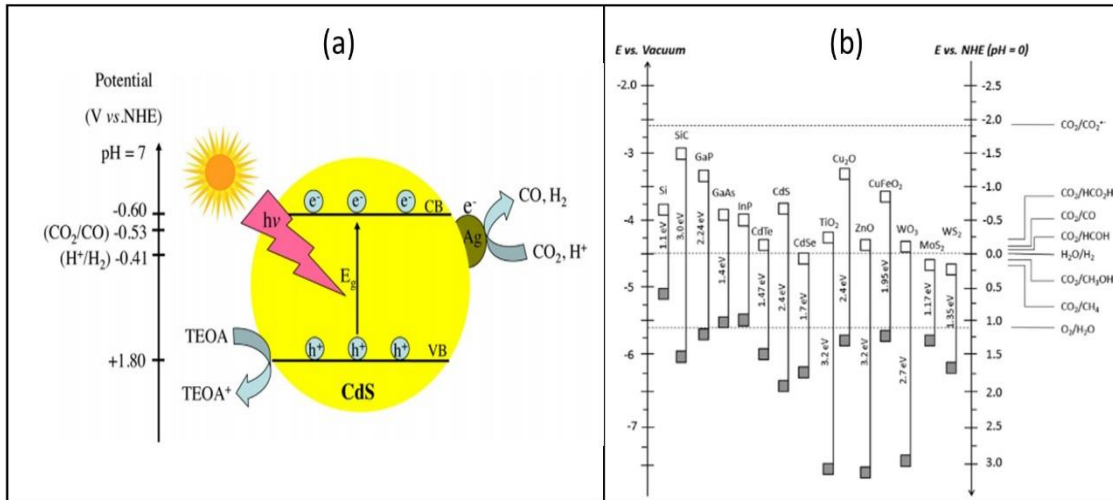


Fig. 1.2 Schematic of CO_2 photocatalytic reduction on a semiconductor photocatalyst (a) Reprinted from ref. [18] Copyright (2017), with permission from Elsevier; Conduction band and valence band potentials of some commonly used semiconductors, with the potentials of several CO_2 and water redox couples at pH 0, plotted versus vacuum and normal hydrogen electrode (NHE) (b) Reprinted (adapted) with permission from [6] Copyright (2015) American Chemical Society.

However, photocatalysis on semiconductors meets difficulties as well. On one hand, the band gap of common semiconductors like TiO_2 , ZnO , WO_3 are approaching 3 eV, which hinders the absorption of large proportion of solar spectrum. On the other hand, even with smaller band gap semiconductors (less than 1.3 eV), maximum solar conversion efficiency is at the Shockley–Queiesser limit around 30% [23]. Therefore, recent development aims at improving efficiency of photocatalysis, which combines multiple semiconductors [24] or more focuses on nanostructure techniques [25]. Although some efforts of optimization have already been made, there are still several aspects that has been left unexplored.

(3) Electrochemical reduction of CO₂

In contrast to above methods of CO₂ conversion, electrochemical reduction of CO₂ is easy to be controlled under rather mild environment and would provide good selectivity of production. Moreover, the electric energy used in CO₂ conversion could be obtained through renewable energy, like solar and wind. Thus, electrochemical reduction process is considered as a novel strategy for converting CO₂.

Nevertheless, there are two main difficulties for electrochemical reduction CO₂ in aqueous electrolyte. The first difficulty is high overpotential (−1.85 V vs standard hydrogen electrode (SHE) [6]) for activating inert CO₂ gas into CO₂ anion radical, as showed in Table 1.1 reaction 1. The second is competition with hydrogen evolution reaction (HER, $E^{0'} = -0.141$ V vs. SHE (V)) in aqueous solution, as showed in Table 1.1 reaction 2.

Table 1.1 Formal Electrochemical Redox Potentials (pH 7) for the Reduction of CO₂ in Aqueous Media [6]

No.	Reaction	$E^{0'}$ vs. SHE (V)
1	$\text{CO}_2 + \text{e}^- \rightarrow \text{CO}_2^{\bullet-}$	−1.85
2	$2\text{H}_2\text{O}_{(l)} + 2\text{e}^- \rightarrow \text{H}_{2(g)} + 2\text{OH}^-_{(aq)}$	−0.414
3	$\text{CO}_{2(g)} + \text{H}_2\text{O}_{(l)} + 2\text{e}^- \rightarrow \text{HCOO}^-_{(aq)} + \text{OH}^-_{(aq)}$	−0.665
4	$\text{CO}_{2(g)} + \text{H}_2\text{O}_{(l)} + 2\text{e}^- \rightarrow \text{CO}_{(g)} + 2\text{OH}^-_{(aq)}$	−0.521
5	$\text{CO}_{2(g)} + 3\text{H}_2\text{O}_{(l)} + 4\text{e}^- \rightarrow \text{HCOH}_{(l)} + 4\text{OH}^-_{(aq)}$	−0.485
6	$\text{CO}_{2(g)} + 5\text{H}_2\text{O}_{(l)} + 6\text{e}^- \rightarrow \text{CH}_3\text{OH}_{(l)} + 6\text{OH}^-_{(aq)}$	−0.399
7	$\text{CO}_{2(g)} + 6\text{H}_2\text{O}_{(l)} + 8\text{e}^- \rightarrow \text{CH}_{4(g)} + 8\text{OH}^-_{(aq)}$	−0.246

The mechanism of CO₂ reduction reaction (CO₂RR) on metal electrodes generally contains two steps [26]. The first step is formation of CO₂ anion radical (CO₂^{•-}) from CO₂ (No.1 reaction in Table 1.1). This step needs a rather high overpotential as -1.85 V vs. SHE (V). Then the second step is converting CO₂^{•-} into products depending on the adsorption status of CO₂^{•-} on electrode [26,27]. Generally speaking, the electrodes with no or low CO₂^{•-} adsorb ability would produce HCOOH (Pb, Hg, In, Sn, etc. known as Group 1 in Fig. 1.3), whilst the other electrodes with higher ability of adsorption would produce CO or higher carbon products (Au, Ag, Zn, etc. known as Group 2; and Cu, etc. known as Group 3 in Fig. 1.3).

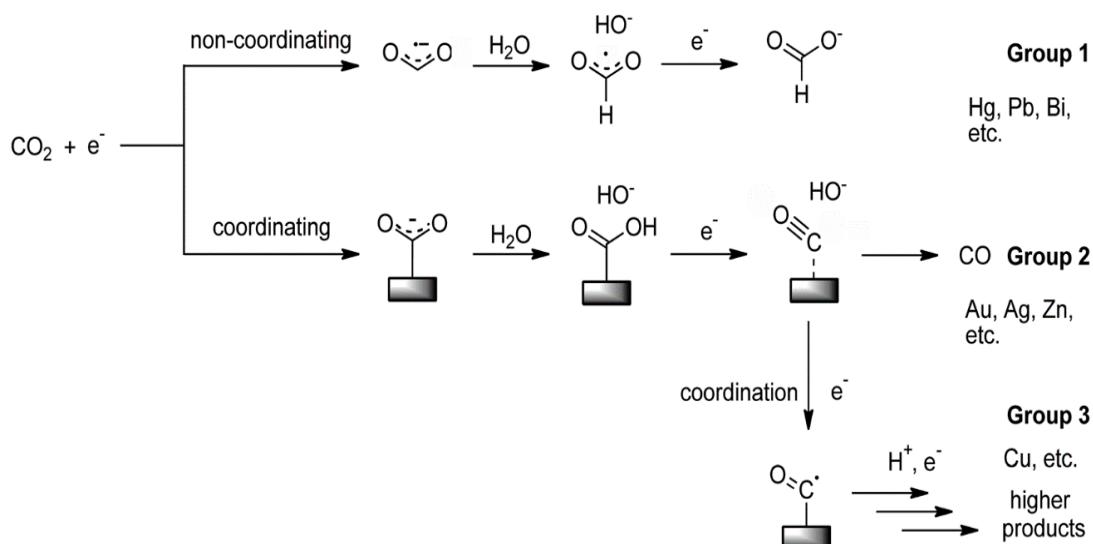


Fig. 1.3 Reaction mechanism of electrochemical reduction of CO₂ on metal electrodes in aqueous solutions. Reprinted from ref. [26] Copyright (2014), with permission from Royal Society of Chemistry.

Nernst Equation $\frac{C_O}{C_R} = \exp\left(\frac{nF(E-E^{0'})}{RT}\right)$ describes the relationship

between the concentrations of oxidized/reduced species (C_O and C_R) and the potential (E). In this equation, $E^{0'}$ is the formal redox potential (Table 1.1), n is the number of electrons used for formation of products by CO₂ reduction, F is Faraday constant (96485 C mol⁻¹), R is the universal gas constant (8.314 J K⁻¹ mol⁻¹), and T is the temperature in kelvins. This equation indicates the

CO₂ reduction could be carried out only when the applied potential is significantly more negative than E^0 . However, the more negative potential is applied, the more HER competition (No.2 reaction in Table 1.1) occurs as well.

For this reason, it is necessary to use appropriate electrode or catalyst for achieving good selectivity of CO₂ reduction. The selectivity of CO₂ reduction is reflected by faradaic efficiency of specific product [8]. Metals, metal oxides and carbon-base materials are widely investigated for CO₂ reduction [5]. Among metal electrodes, Cu-based material is the most investigated one [28]. Various products like CO, CH₄, C₂H₄, and alcohols could be produced in one cell setup by Cu electrodes [29]. It indicated that, CO was obtained at first while further reduction of CO occurred at more negative potential would produce hydrocarbons and alcohols. The selectivity is dependent on the applied potential and electrolyte species. However, unavoidable “deactivation” of electrodes in CO₂ reduction has been reported [30], because of carbonaceous or organic substances formed during the CO₂ reduction poison the reaction.

Besides metal and metal oxide electrodes, carbon-based catalyst become increasingly attractive material for CO₂ reduction. It is so-called carbon solve carbon problem [31]: Nitrogen doped Carbon Nano Tubes (NCNT) catalyst, could convert CO₂ into CO with high selectivity (80%) under rather low overpotential (−0.18 V) [32]; Nitrogen-doped nano-diamond could convert CO₂ into formate and acetate with ~90% Faradaic efficiency [33]; Boron-doped graphene (B-Graphene) could convert CO₂ into formic acid with efficiency of 66% at −1.4 V [34]; Cu-modified boron-doped diamond could convert CO₂ into multiple C₂/C₃ compounds at −1 V [35]. They are representative of graphene-based, carbon nanotube-based, diamond-based catalysts respectively. It is pointed out that, defective site is the key factor for electrochemical reduction of CO₂ on carbon-based catalyst [36–38].

In summary, electrochemical reduction of CO₂ has mainly three advantages than other CO₂ conversion methods. Firstly, comparing to strict requirements of electrode in photocatalysis, which should have proper band gap to making use of visible light, electrode of electrochemical method is relative flexible. Secondly, it has competitive controllability. Such as, high selectivity of specific product can be achieved by adjusting potential [35]; and easy to control electrode surface termination for better selectivity by electrochemical method in the same setting up system [39]. Thirdly, scaleup for industrial application is relatively simple. By simply designing series or parallel electric circuit, electrochemical reduction with large production can be expected.

1.2 Boron doped diamond

1.2.1 Composition of boron-doped diamond (BDD)

Diamond is an insulator with wide band gap of 5.5 eV, while replacing some carbon atoms by heteroatom (like boron, phosphorus or nitrogen), Fermi level would relocated near valence band or conduction band then become semi-conductive. BDD is a p-type semi-conductor, in which boron atoms act as acceptor and provide energy of acceptor (E_A) \sim 0.4 eV near the valence band maxima [40]. Whereas in nitrogen doped and phosphorus doped diamond, nitrogen and phosphorus atom act as donor and provide energy of donor (E_D) at \sim 1.7 eV and \sim 0.6 eV below the conduction band minimum respectively [41]. As the value of E_A is smaller than those of E_D , the p-type BDD has been more practical used than the other diamond materials.

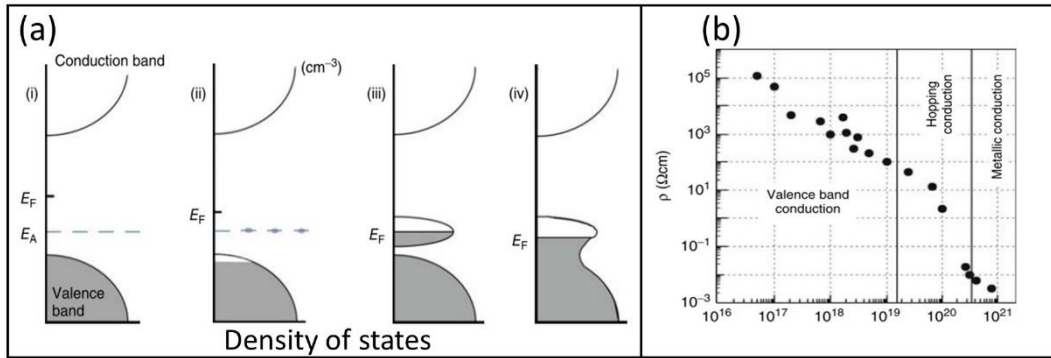


Fig. 1.4 Dependence of Fermi level on boron content (a). Reprinted from ref. [41], Copyright (1969), with permission from Springer Nature. And resistivity changed by increasing boron content (b) Reprinted from ref. [42], Copyright (1998), with permission from Elsevier.

The electrical characters of the BDD electrode are relying on several factors, including boron doping concentration, the presence or absence of sp^2 carbon impurities, surface termination, facet orientation and grain size [43]. In particular, boron content plays an important role. With increasing boron content, Fermi level relocated more closer to the valence band (as showed in Fig. 1.4(a) [41]), thus the conductivity become higher. Based on the resistance value, BDDs are divided into three ranges (in Fig. 1.4(b) [42]). As the boron content [B] in the range of 10^{16} - 10^{19} cm^{-3} , BDD shows valence band conduction as a typical semi-conductor. When the [B] increased to 10^{19} - 10^{20} cm^{-3} , BDD displays hopping conduction of semiconductor. While the [B] is high enough, over 2 - 3×10^{20} cm^{-3} , BDD exhibits metallic conduction [44]. Techniques like secondary ion mass spectroscopy (SIMS) [45], glow discharge optical emission spectroscopy (GDOES) [46] and Raman spectra (half-quantitative) [41] are frequently used to quantify the boron content of BDD.

Sp^2 carbon impurity is another key factor of BDD composition. The pure diamond is composed of sp^3 carbon bond only, while in actually some defected sp^2 carbon formed during manufacturing. Sp^2 carbon is generally

considered to be graphite-like structure (as showed in Fig. 1.5(a) [47]). The sp^2 π bond of graphite structure endows BDD with better conductivity, encourages adsorption through π -interactions, and improves electrocatalytic activity, so that sp^2 -containted-BDD shows good performance in applications of disinfections and ozone production [43,46,48]. Whereas graphite structure is not the only possible structure of sp^2 carbon existence in diamond material, amorphous carbon materials contain sp^3 carbon and sp^2 carbon at the same time, for example diamond like carbon (DLC) possess a significant fraction of sp^3 bonds and some sp^2 carbon (Fig. 1.5(b) [49]). On the country to graphite-like sp^2 carbon materials, amorphous carbon materials expressed rather low conductivity and catalytic activity [50,51]. The analytical methods to identify the fraction of sp^2 and sp^3 species including Raman spectra [52], electron energy loss (EEL) spectroscopy [53] and XPS [54], are widely used in the research of carbon-based materials.

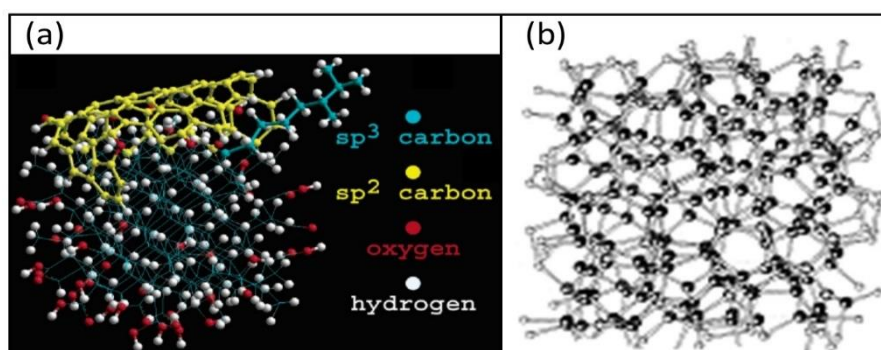


Fig. 1.5 Atomic structure model of sp^2 carbon contained nanodiamond (a) Reprinted (adapted) with permission from ref. [47] Copyright (2006) American Chemical Society. and diamond like carbon (b) [49]

Surface termination of a newly fabricated BDD is usually hydrogen-terminated and hydrophobic (so-called H-BDD). After exposed into air with time, the surface will slowly become oxidized and hydrophilic (so-called O-BDD) [55]. The electron transfer rate on O-BDD is lower than on H-BDD, which is caused by different band position and subsurface band bending [56]. For this reason, BDD pretreatment before application is important. Hydrogen

plasma treatment [57] and cathodic reduction (CR) by electrochemistry method [58] are often used to obtain H-BDD, while oxygen plasma treatment [59] and anodic oxidation (AO) by electrochemistry method [57] are used for getting O-BDD.

Other factors related to the electrical characters like single crystalline or polycrystalline, surface geometry and so on, are as well reported in previous research [41].

1.2.2 Electrochemical properties of BDD

BDD is a promising carbon electrode material, because it has novel electrochemical properties such as wide potential window (showed in Fig. 1.6 [60]), low background current, physical/chemical inertness, and controllable surface termination. In particular, the wide potential window is more prominent than other conventional electrodes. With this wide potential window, many applications can be achieved (see section 1.2.3).

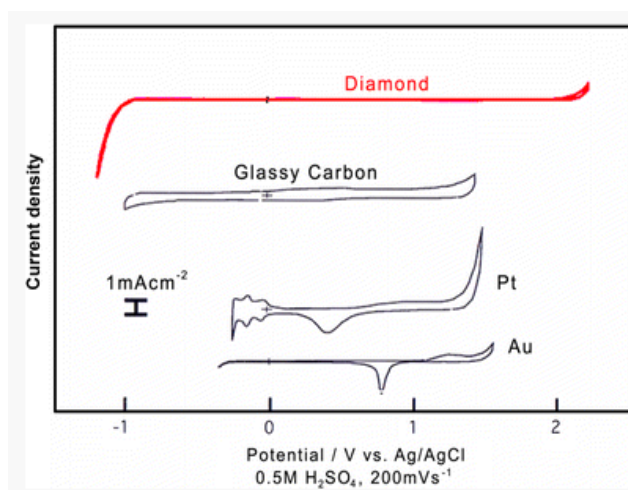


Fig. 1.6 Potential window of BDD and other electrodes. Reprinted from ref. [60], Copyright 2010, with permission from Springer Nature.

The wide potential window of BDD in aqueous solution is due to the hindered water electrolysis, which is caused by a lack of available binding sites on the surface to mediate electron transfer [41]. On the other hand, other electrode materials such as platinum and glassy carbon, unfilled d orbitals and reactive quinone-like groups are present respectively, which enable more effective water–electrode interactions. Thus, BDD possess wider potential window than these electrodes.

1.2.3 Applications of BDD electrode

With remarkable electrochemical properties, in particular wide potential window, BDD electrode has been utilized in the application of electrochemical analysis [61], wastewater treatment [62], organic synthesis [63], CO₂ reduction [64], and Electrogenenerated Chemiluminescence (ECL) [65] with excellent performance.

Electrochemical analysis is the most investigated application of BDD electrode. Inorganic (As³⁺, Pb²⁺, Cd²⁺, Hg²⁺ etc.) and organic (proteins, organic acid, organosulfur compound etc.) compounds could be well detected with BDD electrode [41,60,66]. Comparing with conventional electrodes, BDD refrained interference of water electrolysis at the similar potential due to its wide potential window [67], enhanced signal to noise ratio (S/N) due to its low background current [61], and low fouling due to its low adsorption of contaminants [68]. In consequence, BDD electrodes exhibit remarkable performance of high sensitivity, a low detection limit, and high stability.

1.3 Electrochemical reduction of CO₂ on BDD electrode

So far, the electrochemical reduction of CO₂ on metal electrodes or commercial carbon-based electrode (glassy carbon) are meeting mainly two problems. The first problem is short service life of electrode in ragged environment, like corrosion under high galvanic condition or severe acidic/basic solutions [69], and catalytic behavior deactivated with impurity in electrolyte [70]. The second one is relatively low selectivity of CO₂ reduction, since HER competing with CO₂RR in aqueous solution [71].

In contrast to conventional electrode, diamond electrode exhibited excellent characteristic of corrosion inhibitor in acidic/basic electrolyte [72] and high overpotential [43]. In addition, BDD has a higher overpotential for HER than metal or other carbon materials, thus HER is suppressed with the wide potential window. It indicated that, the dopant-induced active sites can favor CO₂RR over HER [37].

BDD electrode demonstrated satisfactory performance of CO₂RR in the previous studies [71,73]. Formaldehyde was produced in NaCl aqueous solution or seawater as electrolyte [71]. Formic acid was produced in alkaline electrolyte [73]. Methanol was produced in amine electrolyte [72]. Carbon monoxide was produced in KClO₄ electrolyte [74]. Furthermore, higher carbon products were produced on metal-modified BDDs [35,75,76]. Whereas these studies focused primarily on the effect of electrolytes or of the working potential; there has been little investigation of the intrinsic characteristics of BDD electrodes.

1.4 Outline of this thesis

This thesis describes the influence of tailored design of BDD electrodes. Both electrochemical properties and the application of CO₂ reduction affected by this design are discussed. The intrinsic character including boron doping level and sp² impurity content are investigated respectively.

In Chapter 2, the relationship between boron doping level of BDD electrodes and the products of CO₂ reduction is investigated. BDDs with various boron content were manufactured by MPCVD. Structural characterization, electrochemical characterization and electrochemical reduction of CO₂ were conducted. With these investigations, the most proper boron doping level (0.1%) for HCOOH production was found and the heavy doped BDD was proposed to be benefit for producing CO. The research opens new insights for design and control of boron doping level for the electrochemical reduction of CO₂.

In Chapter 3, unexpected phenomena displayed by low-boron-doped BDD electrodes are disclosed. Generally, the presence of sp² nondiamond carbon impurities in BDD electrodes causes undesirable electrochemical properties, such as a reduced potential window and increased background current, etc. However, we found that the potential window and redox reaction in normally doped (1%) BDD and low-doped (0.1%) BDD exhibited opposite tendencies depending on the extent of sp² carbon. Moreover, we found that contrary to the usual expectations, low-doped BDD containing sp² carbon hinders electron transfer, whereas in line with expectations, normally doped BDD containing sp² exhibits enhanced electron transfer. Surface analyses by X-ray/ultraviolet photoelectron spectroscopy (XPS/UPS) and electrochemical methods are utilized to explain these unusual phenomena. This work indicates that the electrochemical properties of low-doped BDD containing sp² are due partially to the high level of surface oxygen, the large work function, the low carrier density, and the existence of different types of sp² carbon.

In Chapter 4, the effect of sp^2 carbon within BDD electrode on the electrochemical reduction of CO_2 is investigated. With increasing sp^2 content, the faradaic efficiency for the production of H_2 under constant current density increases while that for the production of $HCOOH$ decreases. Moreover, favorable electrolysis conditions for producing $HCOOH$ shift in the negative potential direction with increasing sp^2 content. This phenomenon is ascribed to the presence of adsorption sites on the sp^2 carbon. This work provides guidance for selectively controlling of CO_2 reduction by adjusting the distribution of carbonaceous species in the BDD electrode.

1.5 References

- [1] <https://www.esrl.noaa.gov/gmd/ccgg/trends/global.html>. (accessed April 16, 2020).
- [2] WMO, WMO statement on the status of the global climate in 2019, 2020. https://library.wmo.int/doc_num.php?explnum_id=10211. (accessed April 16, 2020).
- [3] C. Song, CO_2 Conversion and Utilization: An Overview, ACS Symp. Ser. 809 (2002) 1–30.
- [4] A. Steele, L.G. Benning, R. Wirth, S. Siljeström, M.D. Fries, E. Hauri, P.G. Conrad, K. Rogers, J. Eigenbrode, A. Schreiber, A. Needham, J.H. Wang, F.M. McCubbin, D. Kilcoyne, J.D. Rodriguez Blanco, Organic synthesis on Mars by electrochemical reduction of CO_2 , *Sci. Adv.* 4 (2018) eaat5118-5127.
- [5] D.D. Zhu, J.L. Liu, S.Z. Qiao, Recent Advances in Inorganic Heterogeneous Electrocatalysts for Reduction of Carbon Dioxide, *Adv. Mater.* 28 (2016) 3423–3452.
- [6] J.L. White, M.F. Baruch, J.E. Pander, Y. Hu, I.C. Fortmeyer, J.E. Park, T. Zhang, K. Liao, J. Gu, Y. Yan, T.W. Shaw, E. Abelev, A.B. Bocarsly, Light-

Driven Heterogeneous Reduction of Carbon Dioxide: Photocatalysts and Photoelectrodes, *Chem. Rev.* 115 (2015) 12888–12935.

[7] E. Alper, O. Yuksel Orhan, CO₂ utilization: Developments in conversion processes, *Petroleum.* 3 (2017) 109–126.

[8] S. Nitopi, E. Bertheussen, S.B. Scott, X. Liu, A.K. Engstfeld, S. Horch, B. Seger, I.E.L. Stephens, K. Chan, C. Hahn, J.K. Nørskov, T.F. Jaramillo, I. Chorkendorff, Progress and Perspectives of Electrochemical CO₂ Reduction on Copper in Aqueous Electrolyte, *Chem. Rev.* 119 (2019) 7610–7672.

[9]https://www.academia.edu/8373516/Thermodynamics_of_the_Urea_Process (accessed April 26, 2020)

[10] J. Wambach, A. Baiker, A. Wokaun, CO₂ hydrogenation over metal/zirconia catalysts, *Phys. Chem. Chem. Phys.* 1 (1999) 5071–5080.

[11] R.M. Morgan-Kiss, J.C. Priscu, T. Pockock, L. Gudynaite-Savitch, N.P.A. Huner, Adaptation and Acclimation of Photosynthetic Microorganisms to Permanently Cold Environments, *Microbiol. Mol. Biol. Rev.* 70 (2006) 222–252.

[12] S.W. Ragsdale, E. Pierce, Acetogenesis and the Wood–Ljungdahl pathway of CO₂ fixation, *Biochim. Biophys. Acta - Proteins Proteomics.* 1784 (2008) 1873–1898.

[13] M. Roger, F. Brown, W. Gabrielli, F. Sargent, Efficient Hydrogen-Dependent Carbon Dioxide Reduction by *Escherichia coli*, *Curr. Biol.* 28 (2018) 140–145.

[14] M. Zhou, S. Wang, P. Yang, C. Huang, X. Wang, Boron Carbon Nitride Semiconductors Decorated with CdS Nanoparticles for Photocatalytic Reduction of CO₂, *ACS Catal.* 8 (2018) 4928–4936.

[15] S. Kumar, R.K. Yadav, K. Ram, A. Aguiar, J. Koh, A.J.F.N. Sobral, Graphene oxide modified cobalt metallated porphyrin photocatalyst for conversion of formic acid from carbon dioxide, *J. CO₂ Util.* 27 (2018) 107–

114.

[16] J. Jin, J. Yu, D. Guo, C. Cui, W. Ho, A Hierarchical Z-Scheme CdS-WO₃ Photocatalyst with Enhanced CO₂ Reduction Activity, *Small*. 11 (2015) 5262–5271.

[17] Inamuddin, A.M. Asiri, E. Lichtfouse, Conversion of Carbon Dioxide into Hydrocarbons Vol. 1 Catalysis, Springer International Publishing, Cham, 2020.

[18] Z. Zhu, J. Qin, M. Jiang, Z. Ding, Y. Hou, Enhanced selective photocatalytic CO₂ reduction into CO over Ag/CdS nanocomposites under visible light, *Appl. Surf. Sci.* 391 (2017) 572–579.

[19] T. Inoue, A. Fujishima, S. Konishi, K. Honda, Photoelectrocatalytic reduction of carbon dioxide in aqueous suspensions of semiconductor powders, *Nature*. 277 (1979) 637–638.

[20] P.-Q. Wang, Y. Bai, P.-Y. Luo, J.-Y. Liu, Graphene-WO₃ nanobelt composite: Elevated conduction band toward photocatalytic reduction of CO₂ into hydrocarbon fuels, *Catal. Commun.* 38 (2013) 82–85.

[21] K. Teramura, S. Iguchi, Y. Mizuno, T. Shishido, T. Tanaka, Photocatalytic conversion of CO₂ in water over layered double hydroxides, *Angew. Chemie Int. Ed.* 51 (2012) 8008–8011.

[22] H. Fujiwara, H. Hosokawa, K. Murakoshi, Y. Wada, S. Yanagida, Surface characteristics of ZnS nanocrystallites relating to their photocatalysis for CO₂ reduction, *Langmuir*. 14 (1998) 5154–5159.

[23] W. Shockley, H.J. Queisser, Detailed balance limit of efficiency of p-n junction solar cells, *J. Appl. Phys.* 32 (1961) 510–519.

[24] H. Li, L. Zhou, L. Wang, Y. Liu, J. Lei, J. Zhang, In situ growth of TiO₂ nanocrystals on g-C₃N₄ for enhanced photocatalytic performance, *Phys. Chem. Chem. Phys.* 17 (2015) 17406–17412.

- [25] M.H. Huang, G. Naresh, H.S. Chen, Facet-Dependent Electrical, Photocatalytic, and Optical Properties of Semiconductor Crystals and Their Implications for Applications, *ACS Appl. Mater. Interfaces*. 10 (2018) 4–15.
- [26] A. Goeppert, M. Czaun, J.-P. Jones, G.K. Surya Prakash, G.A. Olah, Recycling of carbon dioxide to methanol and derived products—closing the loop, *Chem. Soc. Rev.* 43 (2014) 7995–8048.
- [27] Y. Hori, H. Wakebe, T. Tsukamoto, O. Koga, Electrocatalytic process of CO selectivity in electrochemical reduction of CO₂ at metal electrodes in aqueous media, *Electrochim. Acta*. 39 (1994) 1833–1839.
- [28] Y. Hori, CO₂ Reduction Using Electrochemical Approach, in: M. Sugiyama, K. Fujii, S. Nakamura (Eds.), *Sol. to Chem. Energy Convers. Theory Appl.*, Springer International Publishing, Cham, 2016: pp. 191–211.
- [29] Y. Hori, A. Murata, R. Takahashi, Formation of hydrocarbons in the electrochemical reduction of carbon dioxide at a copper electrode in aqueous solution, *J. Chem. Soc. Faraday Trans. 1*. 85 (1989) 2309–2326.
- [30] C.F.C. Lim, D.A. Harrington, A.T. Marshall, Altering the selectivity of galvanostatic CO₂ reduction on Cu cathodes by periodic cyclic voltammetry and potentiostatic steps, *Electrochim. Acta*. 222 (2016) 133–140.
- [31] A. Vasileff, Y. Zheng, S.Z. Qiao, Carbon Solving Carbon's Problems: Recent Progress of Nanostructured Carbon-Based Catalysts for the Electrochemical Reduction of CO₂, *Adv. Energy Mater.* 7 (2017) 1–21.
- [32] J. Wu, R.M. Yadav, M. Liu, P.P. Sharma, C.S. Tiwary, L. Ma, X. Zou, X.D. Zhou, B.I. Yakobson, J. Lou, P.M. Ajayan, Achieving highly efficient, selective, and stable CO₂ reduction on nitrogen-doped carbon nanotubes, *ACS Nano*. 9 (2015) 5364–5371.
- [33] Y. Liu, S. Chen, X. Quan, H. Yu, Efficient Electrochemical Reduction of Carbon Dioxide to Acetate on Nitrogen-Doped Nanodiamond, *J. Am.*

Chem. Soc. 137 (2015) 11631–11636.

[34] N. Sreekanth, M.A. Nazrulla, T.V. Vineesh, K. Sailaja, K.L. Phani, Metal-free boron-doped graphene for selective electroreduction of carbon dioxide to formic acid/formate, *Chem. Commun.* 51 (2015) 16061–16064.

[35] P.K. Jiwanti, K. Natsui, K. Nakata, Y. Einaga, The electrochemical production of C₂/C₃ species from carbon dioxide on copper-modified boron-doped diamond electrodes, *Electrochim. Acta.* 266 (2018) 414–419.

[36] Y. Zhao, G.I.N. Waterhouse, G. Chen, X. Xiong, L.-Z. Wu, C.-H. Tung, T. Zhang, Two-dimensional-related catalytic materials for solar-driven conversion of CO_x into valuable chemical feedstocks, *Chem. Soc. Rev.* 48 (2019) 1972–2010.

[37] J. Wu, T. Sharifi, Y. Gao, T. Zhang, P.M. Ajayan, Emerging Carbon-Based Heterogeneous Catalysts for Electrochemical Reduction of Carbon Dioxide into Value-Added Chemicals, *Adv. Mater.* 31 (2019) 1–24.

[38] Q. Wang, Y. Lei, D. Wang, Y. Li, Defect engineering in earth-abundant electrocatalysts for CO₂ and N₂ reduction, *Energy Environ. Sci.* 12 (2019) 1730–1750.

[39] A. Fujishima, Y. Einaga, T.N. Rao, D.A. Tryk, *Diamond Electrochemistry*, Elsevier B.V., Tokyo, 2005.

[40] J. V. Macpherson, The Use of Conducting Diamond in Electrochemistry, in: *Electrochem. Carbon Electrodes*, 2015: pp. 163–210.

[41] J.P. Lagrange, A. Deneuve, E. Gheeraert, Activation energy in low compensated homoepitaxial boron-doped diamond films, *Diam. Relat. Mater.* 7 (1998) 1390–1393.

[42] T. Watanabe, Y. Honda, K. Kanda, Y. Einaga, Tailored design of boron-doped diamond electrodes for various electrochemical applications with boron-doping level and sp²-bonded carbon impurities, *Phys. Status Solidi.* 211 (2014) 2709–2717.

- [43] K.B. Holt, A.J. Bard, Y. Show, G.M. Swain, Scanning electrochemical microscopy and conductive probe atomic force microscopy studies of hydrogen-terminated boron-doped diamond electrodes with different doping levels, *J. Phys. Chem. B.* 108 (2004) 15117–15127.
- [44] L.A. Hutton, J.G. Iacobini, E. Bitziou, R.B. Channon, M.E. Newton, J. V. Macpherson, Examination of the factors affecting the electrochemical performance of oxygen-terminated polycrystalline boron-doped diamond electrodes, *Anal. Chem.* 85 (2013) 7230–7240.
- [45] T. Watanabe, T.K. Shimizu, Y. Tateyama, Y. Kim, M. Kawai, Y. Einaga, Giant electric double-layer capacitance of heavily boron-doped diamond electrode, *Diam. Relat. Mater.* 19 (2010) 772–777.
- [46] S. Osswald, G. Yushin, V. Mochalin, S.O. Kucheyev, Y. Gogotsi, Control of sp^2/sp^3 carbon ratio and surface chemistry of nanodiamond powders by selective oxidation in air, *J. Am. Chem. Soc.* 128 (2006) 11635–11642.
- [47] I. Duo, A. Fujishima, C. Comninellis, Electron transfer kinetics on composite diamond (sp^3)-graphite (sp^2) electrodes, *Electrochem. Commun.* 5 (2003) 695–700.
- [48] M. Scendo, K. Staszewska-Samson, Effect of Temperature on Anti-Corrosive Properties of Diamond-Like Carbon Coating on S355 Steel, *Materials (Basel)*. 12 (2019) 1659-1673.
- [49] R.L. McCreery, Advanced carbon electrode materials for molecular electrochemistry, *Chem. Rev.* 108 (2008) 2646–2687.
- [50] Y. Tanaka, M. Furuta, K. Kuriyama, R. Kuwabara, Y. Katsuki, T. Kondo, A. Fujishima, K. Honda, Electrochemical properties of N-doped hydrogenated amorphous carbon films fabricated by plasma-enhanced chemical vapor deposition methods, *Electrochim. Acta.* 56 (2011) 1172–1181.

- [51] A. Ferrari, J. Robertson, Interpretation of Raman spectra of disordered and amorphous carbon, *Phys. Rev. B - Condens. Matter Mater. Phys.* 61 (2000) 14095–14107.
- [52] T. Watanabe, S. Yoshioka, T. Yamamoto, H. Sepehri-Amin, T. Ohkubo, S. Matsumura, Y. Einaga, The local structure in heavily boron-doped diamond and the effect this has on its electrochemical properties, *Carbon*. 137 (2018) 333–342.
- [53] O. Romanyuk, M. Varga, S. Tulic, T. Izak, P. Jiricek, A. Kromka, V. Skakalova, B. Rezek, Study of Ni-Catalyzed Graphitization Process of Diamond by in Situ X-ray Photoelectron Spectroscopy, *J. Phys. Chem. C*. 122 (2018) 6629–6636.
- [54] M.C. Granger, M. Witek, J. Xu, J. Wang, M. Hupert, A. Hanks, M.D. Koppang, J.E. Butler, G. Lucazeau, M. Mermoux, J.W. Strojek, G.M. Swain, Standard Electrochemical Behavior of High-Quality, Boron-Doped Polycrystalline Diamond Thin-Film Electrodes, *Anal. Chem.* 72 (2000) 3793–3804.
- [55] Z. Futera, T. Watanabe, Y. Einaga, Y. Tateyama, First principles calculation study on surfaces and water interfaces of boron-doped diamond, *J. Phys. Chem. C*. 118 (2014) 22040–22052.
- [56] T.N. Rao, D.A. Tryk, K. Hashimoto, A. Fujishima, Band-Edge Movements of Semiconducting Diamond in Aqueous Electrolyte Induced by Anodic Surface Treatment, *J. Electrochem. Soc.* 146 (1999) 680–684.
- [57] S. Kasahara, K. Natsui, T. Watanabe, Y. Yokota, Y. Kim, S. Iizuka, Y. Tateyama, Y. Einaga, Surface Hydrogenation of Boron-Doped Diamond Electrodes by Cathodic Reduction, *Anal. Chem.* 89 (2017) 11341–11347.
- [58] J.C. Angus, Y. V Pleskov, S.C. Eaton, Electrochemistry of diamond, in: *Thin Film Diam. II*, Elsevier B.V., 2004: pp. 97–119.
- [59] Y. Einaga, Diamond electrodes for electrochemical analysis, *J. Appl.*

Electrochem. 40 (2010) 1807–1816.

[60] A. Hanawa, K. Asai, G. Ogata, H. Hibino, Y. Einaga, Electrochemical measurement of lamotrigine using boron-doped diamond electrodes, *Electrochim. Acta.* 271 (2018) 35–40.

[61] M.A.Q. Alfaro, S. Ferro, C.A. Martínez-Huitle, Y.M. Vong, Boron doped diamond electrode for the wastewater treatment, *J. Braz. Chem. Soc.* 17 (2006) 227–236.

[62] T. Yamamoto, B. Riehl, K. Naba, K. Nakahara, A. Wiebe, T. Saitoh, S.R. Waldvogel, Y. Einaga, A solvent-directed stereoselective and electrocatalytic synthesis of diisoeugenol, *Chem. Commun.* 54 (2018) 2771–2773.

[63] K. Nakata, T. Ozaki, C. Terashima, A. Fujishima, Y. Einaga, High-yield electrochemical production of formaldehyde from CO₂ and seawater, *Angew. Chemie - Int. Ed.* 53 (2014) 871–874.

[64] Irkham, T. Watanabe, A. Fiorani, G. Valenti, F. Paolucci, Y. Einaga, Co-reactant-on-Demand ECL: Electrogenenerated Chemiluminescence by the in Situ Production of S₂O₈²⁻ at Boron-Doped Diamond Electrodes, *J. Am. Chem. Soc.* 138 (2016) 15636–15641.

[65] J.H.T. Luong, K.B. Male, J.D. Glennon, Boron-doped diamond electrode: Synthesis, characterization, functionalization and analytical applications, *Analyst.* 134 (2009) 1965–1979.

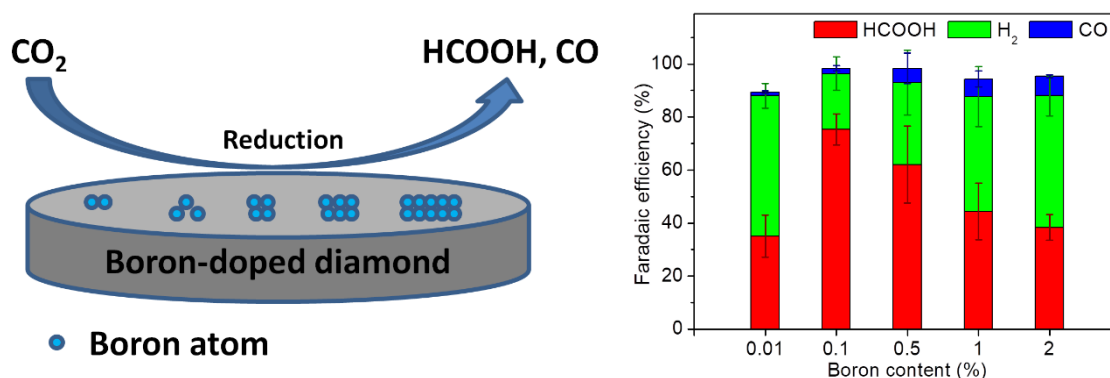
[66] K. Asai, T.A. Ivandini, Y. Einaga, Continuous and selective measurement of oxytocin and vasopressin using boron-doped diamond electrodes, *Sci. Rep.* 6 (2016) 1–10.

[67] E. Diamadopoulou, H. Barndök, N.P. Xekoukoulotakis, D. Mantzavinos, Treatment of ink effluents from flexographic printing by lime precipitation and boron-doped diamond (BDD) electrochemical oxidation, *Water Sci. Technol.* 60 (2009) 2477–2483.

- [68] Q. Chen, G.M. Swain, Structural Characterization, Electrochemical Reactivity, and Response Stability of Hydrogenated Glassy Carbon Electrodes, *Langmuir*. 14 (1998) 7017–7026.
- [69] Y. Hori, Electrochemical CO₂ Reduction on Metal Electrodes, in: *Mod. Asp. Electrochem.*, Springer: New York, 2008: pp. 89–189.
- [70] K. Nakata, T. Ozaki, C. Terashima, A. Fujishima, Y. Einaga, High-yield electrochemical production of formaldehyde from CO₂ and seawater, *Angew. Chemie - Int. Ed.* 53 (2014) 871–874.
- [71] P.K. Jiwanti, K. Natsui, K. Nakata, Y. Einaga, Selective production of methanol by the electrochemical reduction of CO₂ on boron-doped diamond electrodes in aqueous ammonia solution, *RSC Adv.* 6 (2016) 102214–102217.
- [72] K. Natsui, H. Iwakawa, N. Ikemiya, K. Nakata, Y. Einaga, Stable and Highly Efficient Electrochemical Production of Formic Acid from Carbon Dioxide Using Diamond Electrodes, *Angew. Chemie Int. Ed.* 57 (2018) 2639–2643.
- [73] M. Tomisaki, S. Kasahara, K. Natsui, N. Ikemiya, Y. Einaga, Switchable Product Selectivity in the Electrochemical Reduction of Carbon Dioxide Using Boron-Doped Diamond Electrodes, *J. Am. Chem. Soc.* 141 (2019) 7414–7420.
- [74] P.K. Jiwanti, Y. Einaga, Electrochemical reduction of CO₂ using palladium modified boron-doped diamond electrodes: enhancing the production of CO, *Phys. Chem. Chem. Phys.* 21 (2019) 15297–15301.
- [75] P.K. Jiwanti, Y. Einaga, Further Study of CO₂ Electrochemical Reduction on Palladium Modified BDD Electrode: Influence of Electrolyte, *Chem. – An Asian J.* 15 (2020) 910–914.

Chapter 2

Effect of boron doping level on the electrochemical reduction of CO₂ on boron doped diamond electrodes



Reproduced from Xu, J.; Natsui, K.; Naoi, S.; Nakata, K.; Einaga, Y., *Diam. Relat. Mater.*, **2018**, 86, 167-172. with permission from Elsevier.

2.1 Introduction

It is known that the electrochemical characters of the BDD electrode are dependent on several factors such as boron doping level, surface termination, and the presence or absence of sp^2 carbon impurities [1]. In particular, because the boron content determines the electrical conductivity of diamond, it can strongly influence the electrochemical properties [2]. However, no systematic studies exploring the effect of boron content on electrochemical reduction of CO_2 have been made until now. The aim of this chapter is to understand the effect of boron doping content of BDD on the performance for electrochemically reducing CO_2 .

We have reported some results of using BDD as electrode for the electrochemical reduction of CO_2 . These researches focused on the applied potentials and the electrolytes (seawater [3], ammonia [4], and alkaline [5]), but seemed to be insufficient to investigate the characteristics of BDD itself.

For investigating the relationship between the boron content and electrocatalytic ability for reducing CO_2 , five BDD samples with different boron contents were prepared by controlling the ratio of boron source and carbon source.

2.2 Experimental

Five kinds of polycrystalline BDD thin films were grown on Si(100) substrates using microwave plasma-assisted chemical vapor deposition (MPCVD, AX6500X, CORNES Technologies corp.) system according to our previous paper [1]. The boron source, $B(CH_3)_3$, and the carbon source, CH_4 , were supplied into H_2 plasma with a series of B/C atomic ratio of 0.01%, 0.1%, 0.5%, 1%, and 2%. The deposition time was 6 hours.

BDD electrodes were characterized by a scanning electron microscope (SEM), Raman spectroscopy (excited wavelength: 532 nm), and glow discharge optical emission spectroscopy (GDOES). The surface morphology

was observed by SEM (JCM-6000, JEOL). Raman spectra was recorded in ambient air at room temperature with an Acton SP2500 (Princeton Instruments). The actual boron content of each BDD was estimated by GDOES (GD-Profilier2, Horiba Ltd.) with reference to BDD whose boron content was already estimated.

The electrochemical measurements were conducted in two-compartment flow cell separated with Nafion membrane (NRE-212, 0.002in thickness, Aldrich), as described in our previous research [6] with BDD as working electrode, Pt plate as counter electrode, and Ag/AgCl as reference electrode. The geometric areas of both BDD and Pt electrode in the contact with electrolyte were 9.62 cm². Prior to every electrochemical measurement, two steps of electrochemical pretreatment, with which the surface termination of BDD can be consistent, using cyclic voltammetry (CV) in 0.1 M H₂SO₄ aqueous solution were conducted. First step was performed from -3.5 V to +3.5 V for 10 cycles at a scan rate of 1 V s⁻¹ to remove some contaminants from the surface. Second step was performed from 0 V to +3.5 V for 20 cycles at 1 V s⁻¹ to oxidize the BDD surface. To investigate the fundamental electrochemical properties of the BDD electrodes, CV measurements were carried out in 1 mM K₃[Fe(CN)₆] with 1 M KCl aqueous solution with a scan rate of 0.1 V s⁻¹. Moreover, potential windows of the BDD electrodes were examined by CV measurements in 0.1 M H₂SO₄ aqueous solution with a scan rate of 0.1 V s⁻¹. The potential window was defined as the range between anodic and cathodic potentials at which the current density reached ±250 μA cm⁻².

The electrochemical reduction of CO₂ was performed in the following procedure. Catholyte and anolyte were 0.5 M KCl and 1 M KOH aqueous solutions, respectively. The volumes of catholyte and anolyte were 50 mL each. The electrolytes were circulated in the cell by peristaltic pumps with a flow rate of 100 mL min⁻¹. Catholyte was bubbled with N₂ gas for 30min to remove the dissolved oxygen, and then CO₂ gas was bubbled for 1 hour to saturate CO₂. The pH of catholyte was around 6 before electrolysis and

around 8 after electrolysis. After N₂ and CO₂ saturation, linear sweep voltammetry (LSV) measurements were carried out in the potential range from 0 V to -1.8 V at 0.02 V s⁻¹. All the reduction processes were performed with chronopotentiometry method at -2 mA cm⁻² for 1 hour. During reduction, CO₂ was continually bubbled into the catholyte. After the electrolysis, N₂ gas was bubbled into catholyte for 15 min to collect gaseous products into an aluminum bag (CEK 3008-26401, GL Science). The products were analyzed by a gas chromatography (GC) and a high-performance liquid chromatography (HPLC). H₂ and CO were quantitated by GC (GC-2014, Shimadzu Corp.) with thermal conductivity detector (TCD) and flame ionization detector (FID). Formic acid was quantitated by HPLC with electroconductivity detector (Prominence, Shimadzu Corp.). The faradaic efficiency was estimated by following equation (1):

$$\text{Faradaic efficiency (\%)} = nFc/Q \times 100 \quad (1)$$

where n is the number of electrons used for formation of products by CO₂ reduction, F is Faraday constant (96,485 C mol⁻¹), c is the amount of products (mol), and Q is total charge passed in reduction process.

2.3 Results and discussion

2.3.1 Structural characterization of BDD electrodes

The fine polycrystalline structure was observed by SEM (images of all BDD electrodes as shown in Fig. 2.1 [7]). For all five BDDs, the average grain sizes are in the range of 1 to 10 μm. This is similar as previous reports [8,9].

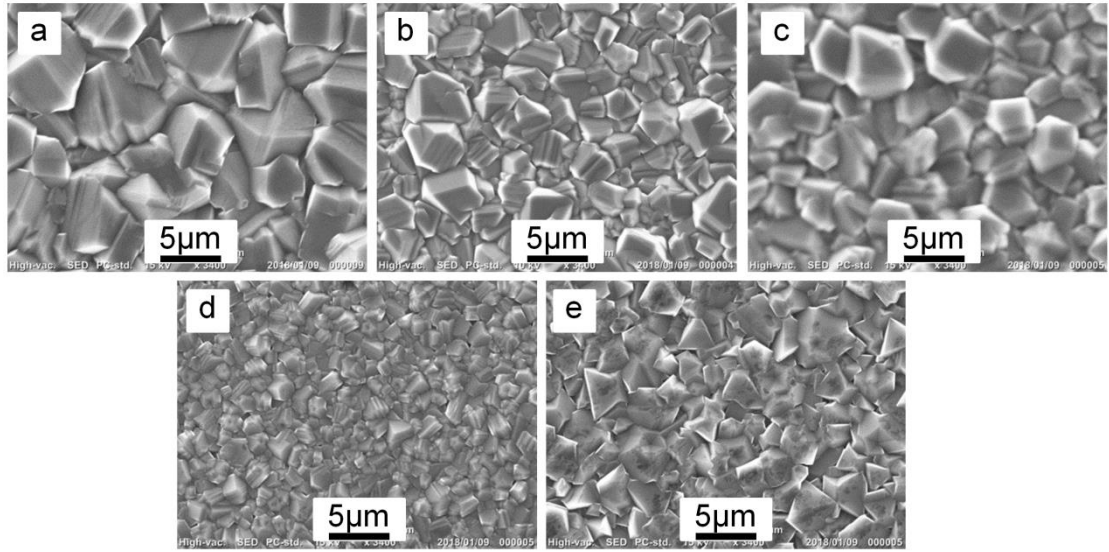


Fig. 2.1 SEM images of BDD electrodes with the boron content of (a) 0.01%, (b) 0.1%, (c) 0.5%, (d) 1%, and (e) 2% at the same magnification. Reproduced from ref. [7], copyright (2018), with permission from Elsevier.

From Raman spectra (Fig. 2.2), the peak derived from the first-order diamond phonon at around 1332 cm^{-1} was observed in all five BDDs [8]. The peak position of first-order diamond phonon lines (ω_D) in BDDs with the boron content of 0.01% and 0.1% (1333 cm^{-1} and 1335 cm^{-1} , respectively) was similar as that in undoped diamond (1332 cm^{-1}). On the contrary, with increasing boron content to 0.5%, 1%, and 2%, the ω_D values were gradually shifted to lower wavenumber (1329 cm^{-1} , 1317 cm^{-1} , and 1305 cm^{-1} , respectively). The shift to lower wavenumber is caused by the tensile stress [10]. In BDD, the boron atoms whose radius is bigger than carbon replace carbon atoms of diamond, which can induce an expansion of diamond lattice and tensile stress. Also, the shift comes from the Fano effect induced by quantum mechanical interference between the discrete phonon and electronic continuum [11]. In addition, Raman spectra of BDDs with high boron content (0.5%, 1%, and 2%) show large bands at around 460 cm^{-1} and 1220 cm^{-1} , which are attributed to the B-B and B-C vibration,

respectively, and moreover, these bands are typically observed in highly boron-doped diamond [8,11]. On the other hand, there is no peak at around 1540 cm^{-1} derived from sp^2 carbon in any BDD films.

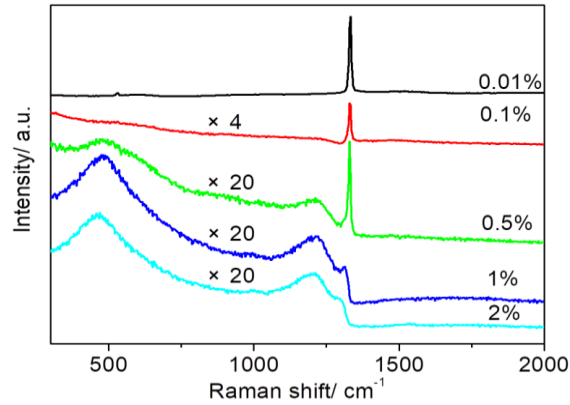


Fig. 2.2 Raman spectra of BDD films with the boron content of 0.01% (black), 0.1% (red), 0.5% (green), 1% (blue), and 2% (light blue). Reproduced from ref. [7], copyright (2018), with permission from Elsevier.

From GDOES analysis, we confirmed the actual boron content in BDD films could be controlled by adjusting B/C ratio in the feed gases (Table 2.1). According to the SEM, Raman spectra, and GDOES results, we confirmed that the five kinds of prepared BDD electrodes have different compositions in terms of boron doping content. The characteristics of the BDD electrodes are summarized in Table 2.1.

Table 2.1 Properties of BDD electrodes with different boron content.

B/C in feed gases (%)	Actual B/C in BDD films (%)	ω_D^* (cm^{-1})
0.01	0.04	1333
0.1	0.19	1335
0.5	0.64	1329
1	1.10	1317
2	2.36	1305

*The peak position of the first-order diamond phonon line from Raman spectra.

2.3.2 Electrochemical properties of BDD electrodes

The potential windows of five BDDs were examined by CV measurements in 0.1 M H₂SO₄ aqueous solution with a scan rate of 0.1 V s⁻¹. The potential window became narrow with increasing boron content (Fig. 2.3), which was in accordance with multiple researches [1,12,13]. It is partly attributed to the lower fraction of exposed grain boundaries. The other is that lower boron doping level leads to decrease in the density of electronic states at negative potentials. As mentioned before, the wider the potential window is, the more suppressively hydrogen generation occurs. In consequence, low boron content would be an advantage for CO₂ reduction.

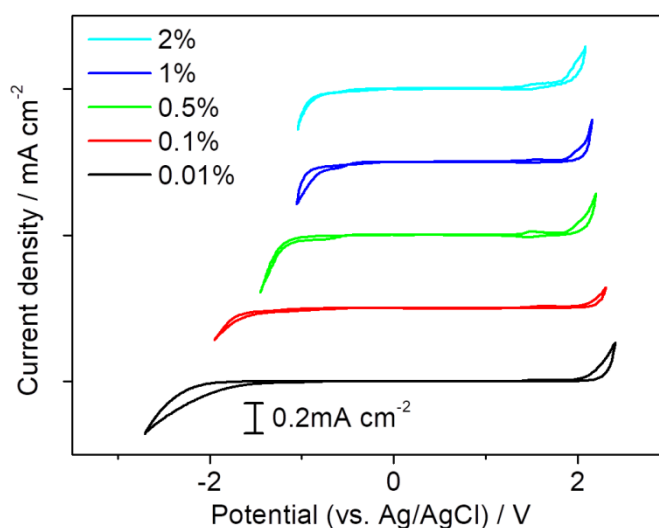


Fig. 2.3 CV curves of BDD electrodes with the boron content of 0.01% (black), 0.1% (red), 0.5% (green), 1% (blue), and 2% (light blue) in 0.1 M H₂SO₄ aqueous solution with a scan rate of 0.1 V s⁻¹. Reproduced from ref. [7], copyright (2018), with permission from Elsevier.

As shown in Fig. 2.4, CV curves of 1 mM K₃[Fe(CN)₆] on BDD electrodes exhibit improvement of reversibility with increasing boron content. The peak-to-peak potential separation (ΔE_p) gradually decreased from 1.317 V to 0.074 V with increasing boron content from 0.01% to 2%.

The smaller ΔE_p indicates higher electrochemical reactivity. This can be explained through the surface microstructure of small size grains as demonstrated by SEM analysis (Fig. 2.1 and Table 2.1) and relatively low resistivity of BDD with high boron doping level. The cathodic/anodic peak currents increased with increasing boron content, which indicated the growth of electrical conductivity. These may be caused by the increase in density of electronic states formed within the band gap of doped diamond as the boron doping level increases [2,14]. This phenomenon has been largely studied as the charge transfer proceeds through a more inner-sphere electron transfer pathway [11,12,14]. It indicated BDD electrode with high boron content has high electrochemical reactivity.

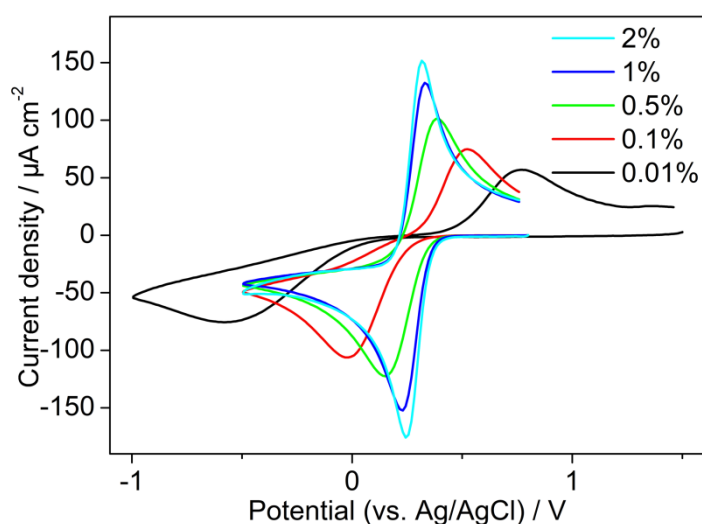


Fig. 2.4 CV curves of BDD with the boron content of 0.01% (black), 0.1% (red), 0.5% (green), 1% (blue), and 2% (light blue) in 1 mM $\text{K}_3[\text{Fe}(\text{CN})_6]$ aqueous solution containing 1 M KCl with a scan rate of 0.1 V s^{-1} . Reproduced from ref. [7], copyright (2018), with permission from Elsevier.

2.3.3 Performance of BDD electrodes for the electrochemical reduction of CO₂

We investigated the performance of five BDD electrodes for the electrochemical reduction of CO₂. Fig. 2.5 shows LSV curves of BDD electrodes with various boron contents in 0.5 M KCl aqueous solution after N₂ and CO₂ saturation. After N₂ saturation (Fig. 2.5a), the cathodic reaction is only related to hydrogen evolution. The current density increased with increasing boron content, indicating the progress of hydrogen evolution, which was in accordance with the narrowing potential window in H₂SO₄ aqueous solution (Fig. 2.3). After CO₂ saturation as shown in Fig. 2.5b, cathodic current caused by not only hydrogen evolution but also CO₂ reduction also increased with increasing boron content. It suggested the reduction reaction was easy to happen on BDD electrodes with higher boron content.

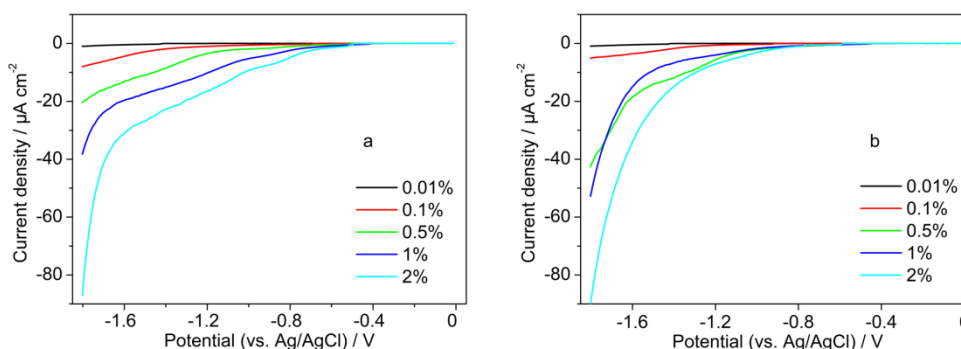


Fig. 2.5 LSV curves of BDD electrodes with the boron content of 0.01% (black), 0.1% (red), 0.5% (green), 1% (blue), and 2% (light blue) in aqueous solutions of 0.5 M KCl as catholyte and 1 M KOH as anolyte with a scan rate of 0.02 V s⁻¹ after (a) N₂ and (b) CO₂ saturation. Reproduced from ref. [7], copyright (2018), with permission from Elsevier.

Electrolysis of CO_2 was carried out on BDD electrodes at -2 mA cm^{-2} for 1 hour. The reduction potential decreased with increasing boron content (Fig. 2.6). This can be ascribed to the decline of resistance by increasing boron content.

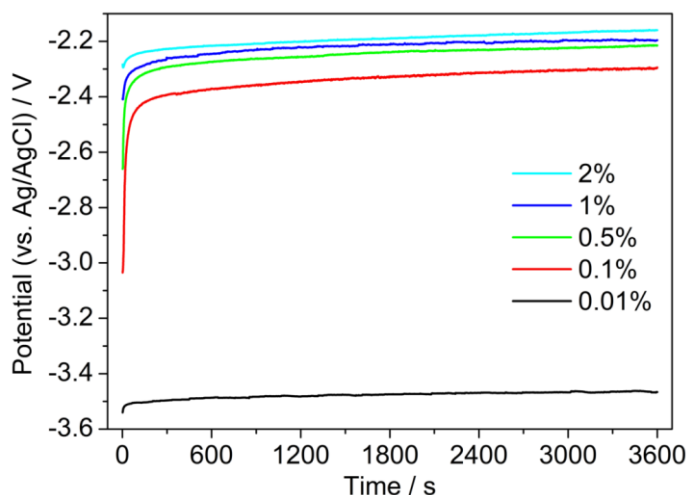


Fig. 2.6 Chronopotentiograms of BDD electrodes with the boron content of 0.01% (black), 0.1% (red), 0.5% (green), 1% (blue), and 2% (light blue) in aqueous solutions of 0.5 M KCl saturated with CO_2 as catholyte and 1 M KOH as anolyte with a flow rate of 100 mL min^{-1} at -2 mA cm^{-2} for 1 h. Reproduced from ref. [7], copyright (2018), with permission from Elsevier.

Fig. 2.7 shows the relationship between the boron content of BDD electrode and the faradaic efficiency for reduction products. Formic acid and hydrogen were the major products, while CO was the minor product. The optimum boron content for formic acid formation was found to be 0.1%. The faradaic efficiency for producing formic acid was the maximum (75%) on BDD electrode with the boron content of 0.1%, and it decreased with increasing boron content. As to the production of CO, the faradaic efficiency slightly increased with increasing boron content, although all faradaic efficiencies for producing CO on five BDD electrodes were below 7%. Meanwhile, the faradaic efficiency for hydrogen evolution was the minimum (21%) on the BDD electrode with the boron content of 0.1%, and it increased

with increasing boron content. As mentioned before, higher boron content leads to progress of hydrogen evolution. Thus, the faradaic efficiency for producing formic acid decreased at higher boron content in favor of hydrogen evolution. At the boron content of 0.01%, the faradaic efficiencies for producing formic acid and CO were the minimum values in all BDD electrodes. This is probably because the electrochemical reactivity is quite low as described above (Fig. 2.4).

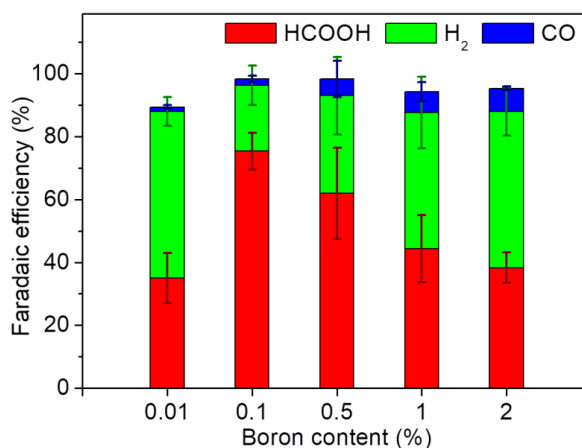
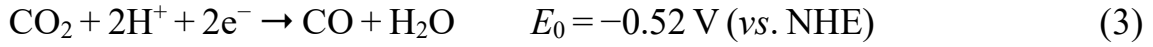
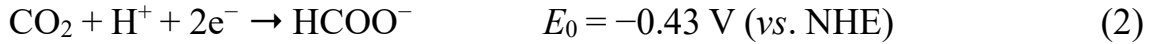


Fig. 2.7 Faradaic efficiencies for producing HCOOH (red), H₂ (green), and CO (blue) of CO₂ reduction on BDD electrodes with various boron contents at -2 mA cm^{-2} for 1 hour. The error bars show the standard deviation obtained by repeating experiments 3 times. Reproduced from ref. [7], copyright (2018), with permission from Elsevier.

2.3.4 Possible mechanism for CO₂ reduction on BDD electrodes with various boron contents

Two compounds as formic acid and CO could be obtained by the electrochemical reduction of CO₂ using BDD electrodes. The mechanisms for the CO₂ reduction to formic acid and CO have been widely reported [15,16]. Two electrons are involved in each of these reactions, which are shown in equation (2) and (3).



The previous researches proposed the reaction pathways of two steps for the electrochemical reduction of CO₂. In the first step, CO₂ is reduced with one electron to CO₂ anion radical (CO₂^{•-}). In the second step, the pathways of forming formic acid and CO from CO₂^{•-} are different, as the former is non-coordinating while the latter is coordinating on electrodes surface [15]. That is, the electrodes, on which CO₂^{•-} can hardly adsorb, mainly produce formic acid. On the other hand, the electrodes, on which CO₂^{•-} can adsorb, mainly produce CO. According to the mechanisms, high faradaic efficiency for producing formic acid could be achieved in this work, probably due to the advantage of chemical inertness and low binding ability of BDD electrode [6].

It is reported that the adsorption of organic materials on BDD electrodes significantly increased with increasing boron doping level [9]. In this case, high boron content BDD is prejudicial for producing formic acid. In contrast, it is preferred for producing CO. In fact, as shown in Fig. 2.7, the faradaic efficiency for producing CO (blue column) increased with increasing boron content, whereas the faradaic efficiency for producing formic acid (red column) decreased in the range of 0.1% to 2%.

Interestingly, the trend of the faradaic efficiency for producing formic acid is coincident with the shift of ω_D from Raman spectra. In heavily doped BDDs, total internal stress increases with increasing boron concentration [8,17]. Moreover, some investigations [10,18] show the electrocatalytic activity of BDD electrodes is related to boron content. Considering the above investigations, the tensile stress in the films, which lead to Raman shift, may be also an important factor for the electrocatalytic activity of the electrodes.

2.4 Conclusion

A series of boron-doped diamond (BDD) electrodes were fabricated by microwave plasma-assisted chemical vapor deposition method with the boron doping level ranging from 0.01% to 2%. These BDD electrodes were used as a working electrode for CO₂ reduction. We obtained formic acid as main product and CO as side product by the electrochemical reduction of CO₂ using BDD electrodes. The best performance for producing formic acid from CO₂ was found on the BDD electrode with the boron content of 0.1%. From the structural characterization and the electrochemical measurements of BDD electrodes, we could observe a dependence of boron doping level on the electrochemical reduction of CO₂. With increasing boron content, the faradaic efficiency for producing formic acid decreased, whereas the faradaic efficiency for hydrogen evolution increased due to narrowing potential window of BDD electrode with high boron content. On the other hand, the faradaic efficiency for producing CO slightly increased with increasing boron content. These trends are probably due to changing the adsorbability and tensile stress of BDD electrodes by different boron doping level. This research opens new insights for design and control of boron-doped diamond for the electrochemical reduction of CO₂.

2.5 References

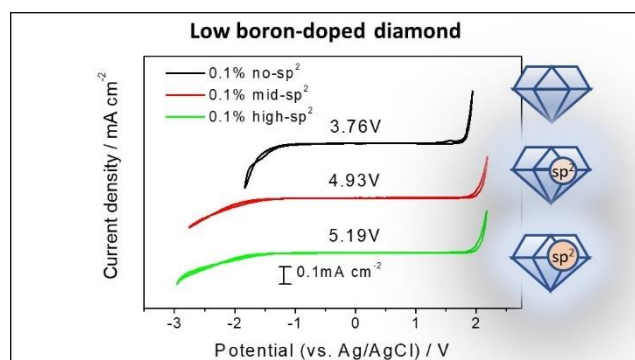
- [1] T. Watanabe, Y. Honda, K. Kanda, Y. Einaga, Tailored design of boron-doped diamond electrodes for various electrochemical applications with boron-doping level and sp²-bonded carbon impurities, *Phys. Status Solidi*. 211 (2014) 2709–2717.
- [2] K.B. Holt, A.J. Bard, Y. Show, G.M. Swain, Scanning electrochemical microscopy and conductive probe atomic force microscopy studies of hydrogen-terminated boron-doped diamond electrodes with different doping levels, *J. Phys. Chem. B*. 108 (2004) 15117–15127.

- [3] K. Nakata, T. Ozaki, C. Terashima, A. Fujishima, Y. Einaga, High-yield electrochemical production of formaldehyde from CO₂ and seawater, *Angew. Chemie Int. Ed.* 53 (2014) 871–874.
- [4] P.K. Jiwanti, K. Natsui, K. Nakata, Y. Einaga, Selective production of methanol by the electrochemical reduction of CO₂ on boron-doped diamond electrodes in aqueous ammonia solution, *RSC Adv.* 6 (2016) 102214–102217.
- [5] N. Ikemiya, K. Natsui, K. Nakata, Y. Einaga, Effect of alkali-metal cations on the electrochemical reduction of carbon dioxide to formic acid using boron-doped diamond electrodes, *RSC Adv.* 7 (2017) 22510–22514.
- [6] K. Natsui, H. Iwakawa, N. Ikemiya, K. Nakata, Y. Einaga, Stable and Highly Efficient Electrochemical Production of Formic Acid from Carbon Dioxide Using Diamond Electrodes, *Angew. Chemie Int. Ed.* 57 (2018) 2639–2643.
- [7] J. Xu, K. Natsui, S. Naoi, K. Nakata, Y. Einaga, Effect of doping level on the electrochemical reduction of CO₂ on boron-doped diamond electrodes, *Diam. Relat. Mater.*, 2018, 86, 167-172.
- [8] R.J. Zhang, S.T. Lee, Y.W. Lam, Characterization of heavily boron-doped diamond films, *Diam. Relat. Mater.* 5 (1996) 1288–1294.
- [9] R. Bogdanowicz, A. Fabiańska, L. Golunski, M. Sobaszek, M. Gnyba, J. Ryl, K. Darowicki, T. Ossowski, S.D. Janssens, K. Haenen, E.M. Siedlecka, Influence of the boron doping level on the electrochemical oxidation of the azo dyes at Si/BDD thin film electrodes, *Diam. Relat. Mater.* 39 (2013) 122–127.
- [10] Y. Feng, J. Lv, J. Liu, N. Gao, H. Peng, Y. Chen, Influence of boron concentration on growth characteristic and electro-catalytic performance of boron-doped diamond electrodes prepared by direct current plasma chemical vapor deposition, *Appl. Surf. Sci.* 257 (2011) 3433–3439.

- [11] K. Schwarzová-Pecková, J. Vosáhllová, J. Barek, I. Šloufová, E. Pavlova, V. Petrák, J. Zavázalová, Influence of boron content on the morphological, spectral, and electroanalytical characteristics of anodically oxidized boron-doped diamond electrodes, *Electrochim. Acta.* 243 (2017) 170–182.
- [12] M.C. Granger, M. Witek, J. Xu, J. Wang, M. Hupert, A. Hanks, M.D. Koppang, J.E. Butler, G. Lucazeau, M. Mermoux, J.W. Strojek, G.M. Swain, Standard Electrochemical Behavior of High-Quality, Boron-Doped Polycrystalline Diamond Thin-Film Electrodes, *Anal. Chem.* 72 (2000) 3793–3804.
- [13] T. Watanabe, T.K. Shimizu, Y. Tateyama, Y. Kim, M. Kawai, Y. Einaga, Giant electric double-layer capacitance of heavily boron-doped diamond electrode, *Diam. Relat. Mater.* 19 (2010) 772–777.
- [14] Ľ. Švorc, D. Jambrec, M. Vojs, S. Barwe, J. Clausmeyer, P. Michniak, M. Marton, W. Schuhmann, Doping Level of Boron-Doped Diamond Electrodes Controls the Grafting Density of Functional Groups for DNA Assays, *ACS Appl. Mater. Interfaces.* 7 (2015) 18949–18956.
- [15] A. Goepfert, M. Czaun, J.-P. Jones, G.K. Surya Prakash, G.A. Olah, Recycling of carbon dioxide to methanol and derived products – closing the loop, *Chem. Soc. Rev.* 43 (2014) 7995–8048.
- [16] D.D. Zhu, J.L. Liu, S.Z. Qiao, Recent Advances in Inorganic Heterogeneous Electrocatalysts for Reduction of Carbon Dioxide, *Adv. Mater.* 28 (2016) 3423–3452.
- [17] K. Bennet, K. Lee, J. Tomshine, E. Sundin, J. Kruchowski, W. Durrer, B. Manciu, A. Kouzani, F. Manciu, Raman Microscopic Analysis of Internal Stress in Boron-Doped Diamond, *Materials (Basel).* 8 (2015) 2782–2793.
- [18] J. Lv, Y. Feng, J. Liu, Y. Qu, F. Cui, Comparison of electrocatalytic characterization of boron-doped diamond and SnO₂ electrodes, *Appl. Surf. Sci.* 283 (2013) 900–905.

Chapter 3

Unusual electrochemical properties of low-doped boron-doped diamond electrodes containing sp^2 carbon



Reprinted (adapted) with permission from Xu, J.; Yokota, Y.; Wong, R.A.; Kim, Y.; Einaga, Y. *J. Am. Chem. Soc.*, **2020**, 142, 2310-2316. Copyright (2020) American Chemical Society.

3.1 Introduction

Generally, BDD containing sp^2 carbon is considered to be low-quality diamond, since, when used as an electrode, it has greater background current [1] and more easily corrodes [2] than high-quality (sp^3) diamond. It was found in previous research that the presence of sp^2 carbon species in highly/normally doped BDD narrowed the potential window in aqueous solutions [3] since this had an effect on the density of states (DOS) in the primary BDD [4,5]. That is, the voltammetric background current, potential window, molecular adsorption, and electron transfer kinetics are affected by the sp^2/sp^3 ratio [6]. Some groups, especially Macpherson et al., have discussed the role of sp^2 species in BDD electrodes including electron transfer processes [7-9]. However, those discussions were limited to BDD with relatively high boron concentrations. Furthermore, fundamental discussions about the surface components and the carrier distributions have been lacking.

BDD electrodes containing sp^2 outperform other electrodes in some specific applications, such as ozone production [1], reduction of concentrated hypochlorite in wastewater [10], electrochemical disinfection [11], and sensors for dissolved oxygen and for measuring pH [12]. Also, highly doped BDD with sp^2 is a promising material for capacitors [13,14]. For p-type boron-doped diamond electrodes, some electrochemical properties were reported [15,16]: the blocking direction of current is cathodic; the asymmetrical current–voltage characteristics have indeed occasionally been observed in redox electrolytes with light doping level; outer-sphere reactions are more reversible than inner-sphere; E^0 is more positive shifted. A gradual change from semiconducting properties to a metallic state is observed as the boron-doping level increases from 10^{16} to 10^{21} cm^{-3} [17]. A value of $2\text{--}3 \times 10^{20} \text{ cm}^{-3}$ is commonly considered as the threshold of semiconducting to metallic [17].

In a previous report, a high faradaic efficiency was found when using a low-boron (0.1%)-doped BDD electrode in the electrochemical reduction of

CO₂ [18,19]. Moreover, taking advantage of the wider potential window, several studies utilizing BDD electrodes with relatively low B/C ratios (1000 ppm [20] and 2500 ppm [21]) for electrochemical analysis have been published. The findings from these studies indicate that not only highly/normally doped BDD but also low-doped BDD has its own advantages in specific fields. Nevertheless, there have been no reports on the influence of the sp² carbon content in low-doped BDD thus far.

In this chapter, we present, the effect of the sp² carbon content on the electrochemical properties of low-doped boron-doped diamond (0.1%). These properties are compared with those of normally doped BDD (1%). Low doping avoids the risks generated in the CVD processes of high-boron-doped diamond. Both low- (0.1%) and normally (1%) doped BDDs were grown with three different sp² levels in order to study how the electrochemical properties change with respect to the sp² content. Moreover, XPS/UPS and Mott–Schottky Plot were used to analyze the surface composition and determine the work function and electron carrier density.

3.2 Experimental

3.2.1 Sample preparation

Six types of polycrystalline BDD films were deposited on Si(100) wafers using a microwave plasma-assisted chemical vapor deposition (MPCVD) reactor (AX6500, CORNES Technologies Corp.). The substrates were pretreated by scratching with diamond powder (~1 μm, Kemet Corp.) and then washed by ultrasonication in isopropyl alcohol. The boron source, B(CH₃)₃, and the carbon source, CH₄, were added to the H₂ plasma. By controlling the boron-to-carbon (B/C) ratio in the gas mixture, two groups of BDD, one with 0.1% boron and one with 1% boron, were prepared using the MPCVD process [19]. Each group involves three different levels of sp² (almost no sp², a middle level of sp², and a high level of sp²), which were

obtained by varying the temperature of the chamber and the flow rate of hydrogen [22]. These samples are designated as 0.1% no-sp², 0.1% mid-sp², 0.1% high-sp², 1% no-sp², 1% mid-sp², and 1% high-sp², respectively.

3.2.2 Characterization

The actual boron content of each BDD sample was estimated by glow discharge optical emission spectroscopy (GDOES, GD-Profilier2, Horiba Ltd.) By GDOES analysis, boron emission intensity (I_B) to carbon emission intensity (I_C) ratio of each BDD sample were achieved and shown in Fig. 3.1 [23]. Comparing to a reference BDD whose boron content had already been estimated by secondary ion mass spectroscopy (SIMS) [14,24], the BDD samples in this text were estimated and listed in Table 3.1. The GDOES data proved that each group (0.1% and 1%) has almost same boron content.

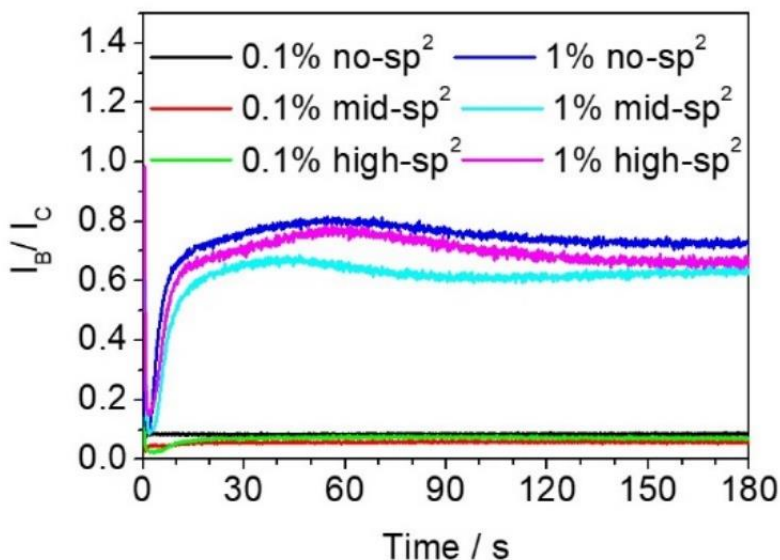


Fig. 3.1 GDOES profiles of 0.1% BDDs (black, red and green) and 1% BDDs (blue, cyan and magenta). Reprinted with permission from ref. [23], Copyright (2020) American Chemical Society.

Table 3.1 Boron content ([B]) estimated by GDOES

	B/C ratio (%)	[B] (cm ⁻³)
0.1% no-sp ²	0.08	1.39×10 ²⁰
0.1% mid-sp ²	0.06	1.0×10 ²⁰
0.1% high-sp ²	0.07	1.21×10 ²⁰
1% no-sp ²	0.74	1.29×10 ²¹
1% mid-sp ²	0.62	1.08×10 ²¹
1% high-sp ²	0.67	1.17×10 ²¹

Table 3.2 Characteristics of the BDD films.

	B% = 0.1 %			B% = 1%		
	no-sp ²	mid-sp ²	high-sp ²	no-sp ²	mid-sp ²	high-sp ²
B/C ratio	0.08	0.06	0.07	0.74	0.62	0.67
grain size (μm)	13.0	10.6	9.5	11.3	8.3	7.3
I_G / I_{Diamond}	0	0.09	0.11	0	0.04	0.15

The surface morphology was observed by SEM (JCM-6000, JEOL). Raman spectra were recorded in ambient air at room temperature with an Acton SP2500 (Princeton Instruments) under excitation at 532 nm from a green laser diode. To compare the relative amounts of sp² carbon in the

different BDD samples, the ratio between the intensities of the G band (around 1530 cm^{-1}) and the diamond band (1332 cm^{-1} for 1% BDDs and 1329 cm^{-1} for 0.1% BDDs) was calculated using Igor software [20]. This ratio is labeled I_G/I_{Diamond} , and the values are given in Table 3.2. Note that the I_G/I_{Diamond} ratio is a qualitative value, not an actual one.

3.2.3 Electrochemical measurement

Cyclic voltammetry (CV) was conducted with a potentiostat (PGSTAT204, MetrohmAutolab) using a homemade single-compartment three-electrode PTFE cell with an Ag/AgCl (saturated KCl) reference electrode (fixed salt bridge) and a fixed 1% BDD plate as the counter electrode. The electrical contacts for electrochemical measurements were made by connecting a copper plate to the BDD surface with silver paste. Before each CV measurement, each BDD electrode was electrochemically pretreated to clean and anodically oxidize (AO) the surface (10 cycles CV scan between potentials of -3.5 and 3.5 V and then 20 cycles CV between potentials of 0 and 3.5 V with a scan rate of 1 V s^{-1} in a $0.1\text{ mol L}^{-1}\text{ H}_2\text{SO}_4$ aqueous solution). The potential windows of the electrodes were examined by CV measurements in $0.1\text{ mol L}^{-1}\text{ H}_2\text{SO}_4$ aqueous solution with a scan rate of 0.1 V s^{-1} . The potential window is defined as the range between the anodic and cathodic potentials at which the current density is under $\pm 250\text{ }\mu\text{A cm}^{-2}$. To investigate the electron transfer performance of the BDD electrodes, CV measurements were carried out in $1\text{ mmol L}^{-1}\text{ K}_3[\text{Fe}(\text{CN})_6]$, $1\text{ mmol L}^{-1}[\text{Ru}(\text{NH}_3)_6]\text{Cl}_3$, and $1\text{ mmol L}^{-1}\text{ Fe}(\text{ClO}_4)_3$ in $1\text{ mol L}^{-1}\text{ KCl}$ aqueous solutions at a scan rate of 0.1 V s^{-1} . Mott–Schottky plots were measured with a potentiostat (ModuLab XM, Solartron Analytical) at a frequency of 5000 Hz in $0.1\text{ mol L}^{-1}\text{ H}_2\text{SO}_4$ solution.

3.2.4 Photoelectron spectroscopy measurement

X-ray/ultraviolet photoelectron spectroscopy (XPS/UPS) (Theta probe, Thermo Fisher Scientific) utilizing a monochromatic Al K α X-ray source (1486.6 eV) and He I UV source (21.2 eV) was carried out in a ultrahigh-vacuum (UHV) chamber with a base pressure of $\sim 10^{-7}$ Pa. The binding energies from the XPS measurements are referenced to the Au 4f $_{7/2}$ peak at 84.0 eV. The XPS data confirmed that the surfaces of the BDD electrodes were free from contamination by the electrolyte (i.e., SO $_4^{2-}$, not shown in present text). The C 1s spectra were deconvoluted into mixed Gaussian–Lorentzian functions using Thermo Scientific Avantage Software. The Shirley background was subtracted from the spectra. Five peaks deconvoluted from the C 1s spectra were assigned to the following components: 282.8 eV (sp 2 C–C), 284.1 eV (C–H bond), 284.75 eV (sp 3 C–C), 285.2 eV (C–O bond), and 286.2 eV (C=O bond). These binding energies were fixed for all the analyses. The B 1s spectra were analyzed to confirm the boron content on the surfaces. The UPS spectra were referenced to the Fermi edge of Au at 0 eV. To resolve the secondary electron cutoff of UPS, a bias voltage of –12 V was applied.

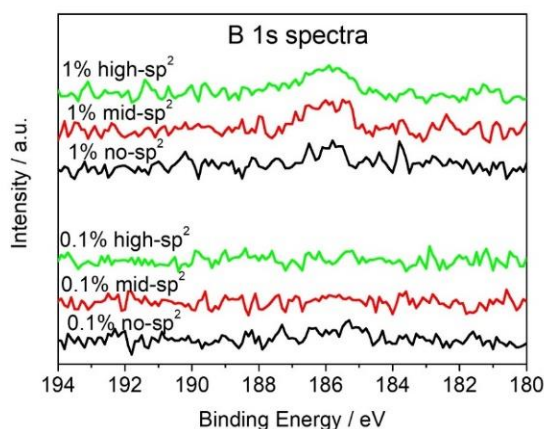


Fig. 3.2 B 1s spectra for a BDD electrodes. Reprinted with permission from ref. [23], Copyright (2020) American Chemical Society.

3.3 Results and discussion

3.3.1 Characteristics

Table 3.2 summarizes the characteristics of all six types of fabricated BDD samples. The six samples can be separated into two groups based on boron concentration, which are B% = 0.1% and B% = 1%. The actual B/C ratio was investigated by GDOES analysis (described in Fig. 3.1). In the group of B% = 0.1%, the actual B/C ratio of no-sp², mid-sp², and high-sp² sample was 0.08%, 0.06%, and 0.07% respectively. On the other hand, the B% = 1% samples displayed actual B/C ratio of no-sp², mid-sp², and high-sp² as 0.74%, 0.62%, and 0.67%, respectively. Boron narrow scan of XPS spectra also played as a qualitative confirmation (Fig. 3.2).

The qualitative value of I_G/I_{Diamond} ratio was estimated by Raman spectroscopy. With the I_G/I_{Diamond} value, the BDD samples of each boron group would be defined as no-sp², mid-sp², and high-sp² BDD. The average grain size estimated by SEM will be discussed in the following text.

A fine polycrystalline structure was observed in the SEM images of all six BDD electrodes as shown in Fig. 3.3. In both series, 0.1% (Fig. 3.3a, b, c) and 1% (Fig. 3.3d, e, f) BDD, the average grain size reduces with increasing sp² content. Also, there are more boundaries in BDD containing sp². This is consistent with previous reports that found sp² is predominantly in the boundaries [24]. Note that the surface areas indicated by atomic force microscopy (AFM) are almost the same whether sp² is present or absent in the BDD [25]. Therefore, the radical changes in the electrochemical properties cannot be ascribed to the difference in surface area of the electrodes. Additionally, there is a higher proportion of (111) facets on the specimens containing sp² than on the sp²-free diamond. This indicates that secondary nucleation increases with sp² [5].

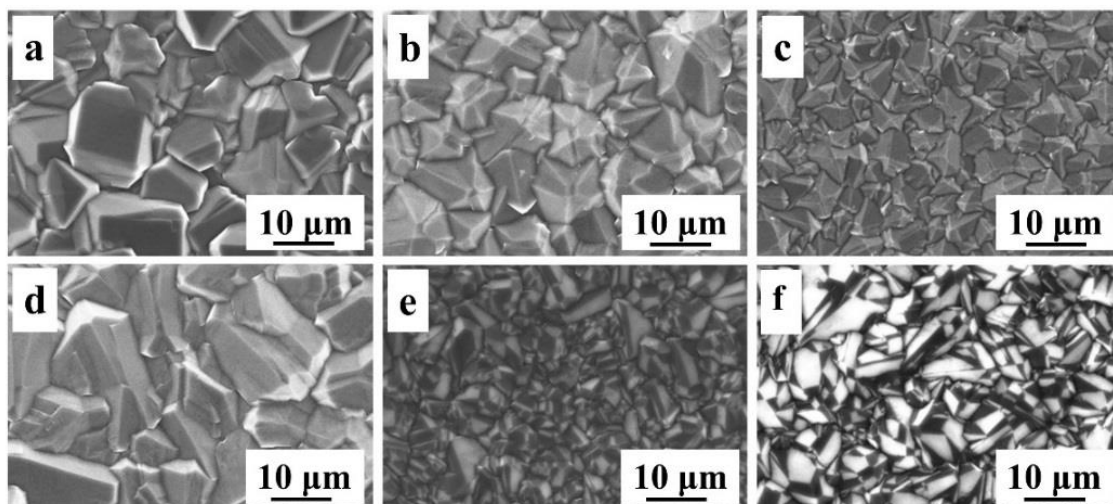


Fig. 3.3 SEMs of fabricated BDD samples. (a), (b), and (c) show images of 0.1% no-sp², 0.1% mid-sp², and 0.1% high-sp² BDD; (d), (e), and (f) show 1% no-sp², 1% mid-sp², and 1% high-sp² BDD. Reprinted with permission from ref. [23], Copyright (2020) American Chemical Society.

In Fig. 3.4, the Raman spectra of all the electrodes show sharp peaks of the zone center phonon line (referred to as the “ZCP”) of diamond. The ZCP peaks of 0.1% BDDs (Fig. 3.4a) are at 1332 cm⁻¹, whereas for 1% BDDs (Fig. 3.4b), they are at 1329 cm⁻¹. This shift is caused by the Fano effect and is consistent with previous reports [24,26]. In addition to the ZCP, there are two Lorentzian peaks referred to as “L1” and “L2” located around 500 and 1200 cm⁻¹, which present as weak bands in Fig. 3.4a and strong asymmetric peaks in Fig. 3.4b. These were classified as being due to metallic and semiconducting materials. The peak around 1530 cm⁻¹ is known as the G band, which is due to bond stretching of sp² atoms in both rings and chains [27].

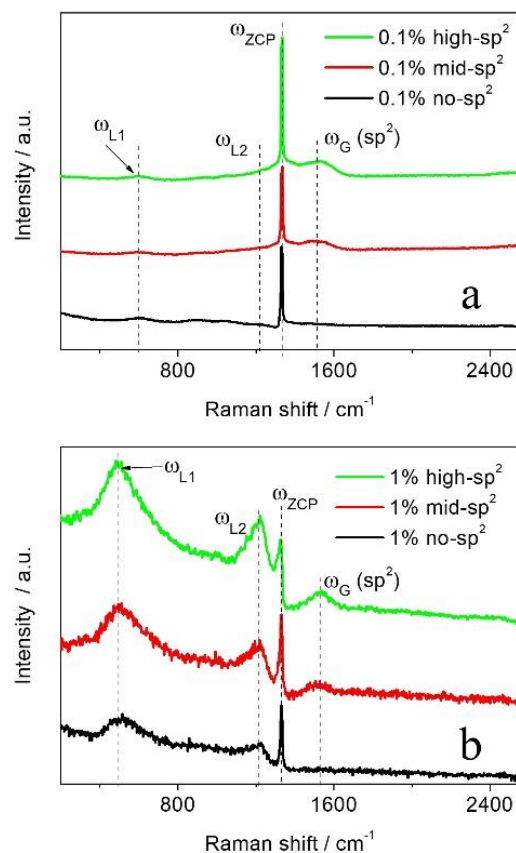


Fig. 3.4 Raman spectra of 0.1% BDDs (a) and 1% BDDs (b). Reprinted with permission from ref. [23], Copyright (2020) American Chemical Society.

Furthermore, the peak shape and position of the G bands for 0.1% BDD are slightly different from those for 1% BDD, as shown in Fig. 3.4. Narrow peaks at 1530 cm⁻¹ were found for 1% mid-sp² and 1% high-sp² BDD, whereas for the 0.1% mid-sp² and 0.1% high-sp² samples, broad peaks at 1515 cm⁻¹ were observed. The broader red-shifted G band of 0.1% BDDs indicated the existence of amorphous carbon on 0.1% BDDs [28,29]. Based on the peak positions of the G band, it was surmised that different types of sp² carbon might be present in 1% BDDs and 0.1% BDD. It is almost all graphite in 1% BDD, whereas it is a mixture of amorphous carbon and graphite in 0.1% BDD.

3.3.2 Electrochemical Properties

Potential Window

Fig. 3.5 shows the potential window (defined as when the current response reaches $\sim\pm 250 \mu\text{A cm}^{-2}$) obtained in $0.1 \text{ M H}_2\text{SO}_4$ aqueous solution using the six different electrodes. The potential windows of the 0.1% BDD electrodes (larger than 3.76 V) are wider than those of the 1% BDD electrodes (smaller than 3.47 V). This indicates that the difference in the electrochemical behavior of the BDD electrodes is mainly due to the difference in boron concentration [28]. Furthermore, as the sp^2 content increases from no- sp^2 to mid- sp^2 and high- sp^2 , the potential window for the 1% BDD electrodes tends to narrow, from 3.47 to 3.37 and 3.33 V , respectively. This is in accordance with common knowledge since the DOS of the primary BDD is affected by the sp^2 content [25]. However, the opposite tendency was observed for 0.1% BDD, which exhibited widening of the potential window from 3.76 to 4.93 and 5.19 V for no- sp^2 to mid- sp^2 and high- sp^2 . The different tendencies between the 1% and 0.1% BDD might be due to the different structure of the sp^2 carbon present in them.

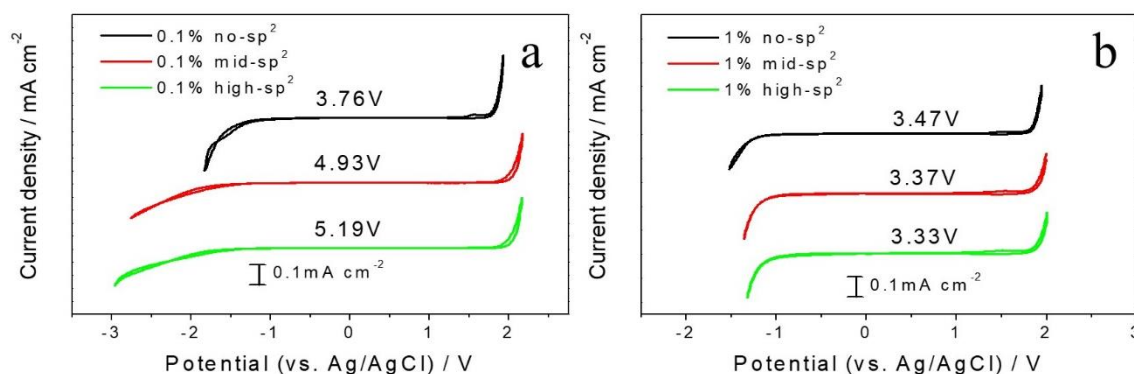


Fig. 3.5 Potential window of 0.1% BDDs (a) and 1% BDDs (b) in $0.1 \text{ mol L}^{-1} \text{ H}_2\text{SO}_4$, scan rate 0.1 V s^{-1} . Reprinted with permission from ref. [23], Copyright (2020) American Chemical Society.

Redox Reactions

Cyclic voltammograms of the six films (Fig. 3.6) were recorded for 1 mmol L⁻¹ [Ru(NH₃)₆]Cl₃ (Fig. 3.6a), 1 mmol L⁻¹ K₃[Fe(CN)₆] (Fig. 3.6b), and 1 mmol L⁻¹ Fe(ClO₄)₃ (Fig. 3.6c), respectively, in 0.5 mol L⁻¹ KCl solutions at a scan rate of 0.1 V s⁻¹. [Ru(NH₃)₆]^{3+/2+} undergoes outer-sphere electron transfer, and the electrode kinetics are relatively insensitive to the surface chemical properties of diamond; [Fe(CN)₆]^{3-/4-} and Fe^{3+/2+} proceeded through inner-sphere electron transfer (slower than outer-sphere), and the electrode kinetics are highly sensitive to the surface termination of diamond.(24) A summary of the electrochemical responses, peak potential separations (ΔE_p), cathodic peak currents (I_c), and expected E^0 value against reference electrode Ag/AgCl on semiconducting/semimetallic BDD is presented in Table 3.3.

The voltammetric data presented above reveal that the effect of increasing the amount of sp² in semiconducting 0.1% BDD and semimetallic 1% BDD has opposite tendencies. Namely, for the 1% BDD samples, the redox reaction kinetics increase with increasing amount of sp² carbon species. It has been widely reported that sp² acts as a catalyst for some reactions [1] and that the density of states is affected [4,5]. Nevertheless, on 0.1% BDDs, the redox reaction is inhibited as the sp² ratio increases, which is contrary to the generally held expectations for highly doped BDD.

First, the CV curves in the [Ru(NH₃)₆]Cl₃ redox system (Fig. 3.6a) exhibited quasi-reversible behavior on 1% BDDs and 0.1% no-sp² BDD. The rate of the redox reaction is relatively insensitive to the surface microstructure, surface oxide, and adsorbed monolayers on sp² carbon electrodes [28]. The values of ΔE_p and I_c on each curve of the 1% BDD electrodes (dashed lines) are similar, being 0.09 V and 160 $\mu\text{A cm}^{-2}$, respectively. This indicates that the surface charge carriers had not been impaired [9] and the density of electronic states near the formal potential of the redox system remained constant [28]. The electron transfer kinetics were extracted from these data (as follows). However, ΔE_p increases with

increasing sp^2 content on 0.1% BDD electrodes (solid lines), from 0.14 V for no- sp^2 to 0.38 V for the mid- sp^2 sample. The CV for the 0.1% BDD high- sp^2 sample was irreversible and lacked an anodic peak, which indicates that there might be an insufficient density of electronic states present within the bandgap at this potential [28]. The current density with the 0.1% BDD electrodes reduces significantly as the amount of sp^2 increases, dropping from $148 \mu\text{A cm}^{-2}$ for no- sp^2 to $106 \mu\text{A cm}^{-2}$ for mid- sp^2 and $26 \mu\text{A cm}^{-2}$ for high- sp^2 . This phenomenon is likely due to domains where the charge carrier concentration or mobility is lower [30].

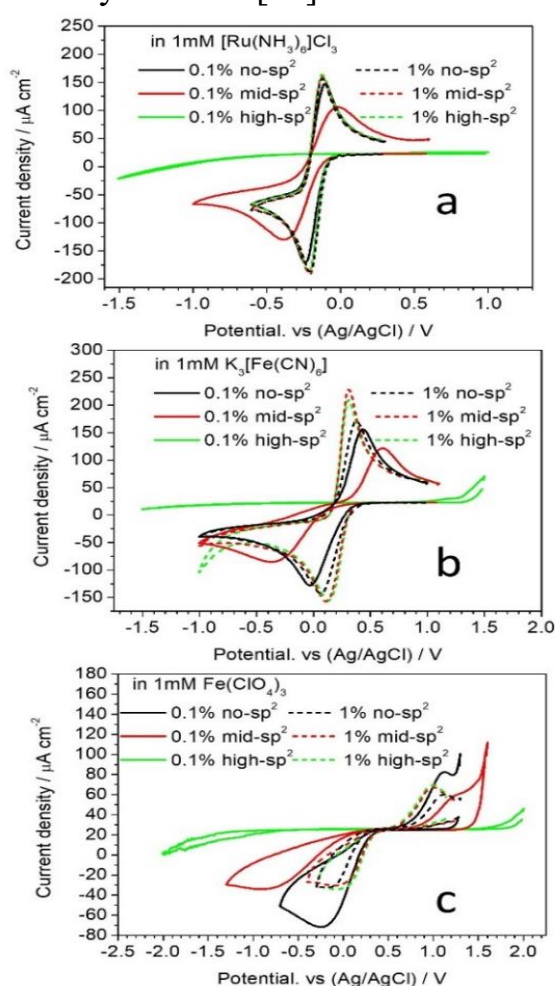


Fig. 3.6 Cyclic voltammograms performed on 0.1% BDD and 1% BDD electrodes at a scan rate of 0.1 V s^{-1} for $1 \text{ mmol L}^{-1} [\text{Ru}(\text{NH}_3)_6]\text{Cl}_3$ (a), $\text{K}_3[\text{Fe}(\text{CN})_6]$ (b), and $\text{Fe}(\text{ClO}_4)_3$ (c), in $0.5 \text{ mol L}^{-1} \text{ KCl}$ solution. Reprinted with permission from ref. [23], Copyright (2020) American Chemical Society.

Table 3.3 Peak Potential Separation and Cathodic Peak Current of the BDD Films in $[\text{Ru}(\text{NH}_3)_6]\text{Cl}_3$, $\text{K}_3[\text{Fe}(\text{CN})_6]$ and $\text{Fe}(\text{ClO}_4)_3$ and Expected E^0 Value in Three Redox Solutions

	B% = 0.1%			B% = 1%			E^0 (V vs. Ag/AgCl)
	no-sp ²	mid-sp ²	high-sp ²	no-sp ²	mid-sp ²	high-sp ²	
$[\text{Ru}(\text{NH}_3)_6]\text{Cl}_3$	ΔE_p (V)	0.14	0.38	-	0.09	0.09	0.09
	I_c ($\mu\text{A cm}^{-2}$)	148	106	26	157	160	164
							-0.099
$\text{K}_3[\text{Fe}(\text{CN})_6]$	ΔE_p (V)	0.47	0.98	-	0.31	0.21	0.18
	I_c ($\mu\text{A cm}^{-2}$)	156	122	30	171	228	209
							0.159
$\text{Fe}(\text{ClO}_4)_3$	ΔE_p (V)	1.37	2.11	-	1.26	1.09	1.07
	I_c ($\mu\text{A cm}^{-2}$)	82	58	-	60	67	69
							0.572

Second, Fig. 3.6b shows the CV curves in $\text{K}_3[\text{Fe}(\text{CN})_6]$ solution with the quasi-reversible and irreversible response. This involves more complex surface-sensitive electron transfer rates, which are highly sensitive to the surface morphology and termination but are relatively insensitive to the presence of sp².(2) On 1% BDD electrodes (dashed lines), ΔE_p decreases proportionally with increasing sp² content, from 0.31 V for the no-sp² sample to 0.21 V for the mid-sp² sample and 0.18 V for the high-sp² sample, and the

current densities are similar at around $200 \mu\text{A cm}^{-2}$. This indicates that the surface oxide species might be slightly different. In contrast, on 0.1% BDD electrodes (solid lines), ΔE_p increases with increasing sp^2 content, from 0.47 V for the no- sp^2 sample to 0.98 V for the mid- sp^2 sample, which demonstrates that the oxidized functional groups on the surface are very much different. There is no anodic peak with the 0.1% high- sp^2 BDD electrode, which is similar to the result with the $[\text{Ru}(\text{NH}_3)_6]^{3+/2+}$ redox system. This characteristic can be ascribed to the p-type semiconducting properties [15], which are related to the surface states and the distribution of electrochemically active sites [30]. The value of I_c on the 0.1% BDD electrode reduces from $156 \mu\text{A cm}^{-2}$ for the no- sp^2 sample to $122 \mu\text{A cm}^{-2}$ for the mid- sp^2 sample and $30 \mu\text{A cm}^{-2}$ for the high- sp^2 sample, which can be ascribed to the change in surface termination.

Third, the irreversible and sluggish kinetics in the CV curves of $\text{Fe}(\text{ClO}_4)_3$ are shown in Fig. 3.6c. The electrode kinetics for $\text{Fe}^{3+/2+}$ are highly sensitive to the presence of oxides on the sp^2 carbon electrodes. The electron transfer for this system might be catalyzed by special chemical interactions with carbonyl groups [31]. As for the 1% BDD electrodes (dashed lines), the ΔE_p values drop slightly from 1.26 to 1.09 and 1.07 V with increasing sp^2 content. The smaller value of ΔE_p shows that it has higher electrochemical reactivity compared to sp^3 BDD [7], and this can be ascribed to oxidized sp^2 carbon catalyzing electron transfer reactions. The corresponding values of I_c increase slightly from 60 to 67 and 69 $\mu\text{A cm}^{-2}$, which is probably due to the impact of sp^2 on the electrode reaction kinetics of certain redox systems [5]. However, on 0.1% BDDs (solid lines), the value of ΔE_p increases and that of I_c decreases with increasing sp^2 content, from 1.37 V and $82 \mu\text{A cm}^{-2}$ for no- sp^2 to 2.11 V and $58 \mu\text{A cm}^{-2}$ for the mid- sp^2 sample. Neither an anodic nor cathodic peak appears with the 0.1% high- sp^2 BDD electrode, which might be due to the extremely sluggish kinetics caused by the absence of mediating surface carbonyl functionalities [28].

On the other hand, the electron transfer kinetics could be extracted from the value of peak separation, which is shown in Table 3.3. According to a simplified work [32] of Nicholson method [33], the heterogeneous electron transfer rate constant can be estimated by equation (1) and (2).

$$\psi = k^0 [\pi D n F v / RT]^{-\frac{1}{2}} \quad (1)$$

$$\psi = (-0.6288 + 0.0021X) / (1 - 0.017X) \quad (2)$$

In which, $D=8.8 \times 10^{-6} \text{ cm}^2 \text{ s}^{-1}$ is diffusion coefficients of $[\text{Ru}(\text{NH}_3)_6]\text{Cl}_3$ [33], $n=1$ is the number of electrons transferred, F is the Faraday constant, R is the molar gas constant, and T is the absolute temperature. The calculated value of $k^0= 0.0086 \text{ cm s}^{-1}$ (1% no- sp^2) and $k^0= 0.0025 \text{ cm s}^{-1}$ (0.1% no- sp^2) respectively. The value of 1% BDD is comparable with the data showed in Swain's paper [28], where is 0.01 cm s^{-1} .

3.3.3 Surface Analysis

To explain the unexpected inactive electrochemical properties on the 0.1% BDD electrodes with sp^2 carbon defects (0.1% mid- sp^2 and 0.1% high- sp^2 samples), XPS measurements were performed to check the composition of the surface. Fig. 3.7 shows deconvoluted C 1s spectra of the six BDD samples. Fitting of the observed spectra was conducted on the basis of the fixed conditions described in the Experimental Section. The relative abundances of the components are summarized in Table 3.4.

Table 3.4 Relative Abundance (%) of the Carbon Components in Each BDD Sample

	1	2	3	4	5
	sp ²	C–H	sp ³	C–O	C=O
	C–C		C–C		
0.1% no-sp ²	0.0	3.1	57.9	35.0	4.0
0.1% mid-sp ²	1.6	3.4	13.6	74.4	7.0
0.1% high-sp ²	4.0	1.4	0.8	88.0	5.9
1% no-sp ²	0.0	7.1	36.7	37.5	18.7
1% mid-sp ²	0.4	10.5	43.5	35.2	10.3
1% high-sp ²	0.8	12.2	43.7	33.3	10.0

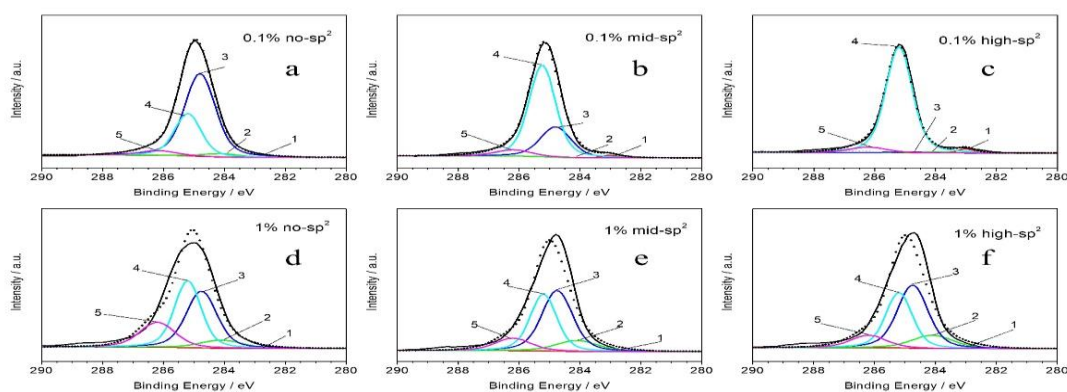


Fig. 3.7 Deconvoluted XPS C 1s spectra for 0.1% BDD electrodes (a–c) and 1% BDD electrodes (d–f). The components are shown as follows: (1) sp² C–C (282.8 eV, red), (2) C–H (284.1 eV, green), (3) sp³ C–C (284.75 eV, blue), (4) C–O (285.2 eV, cyan), and (5) C=O (286.2 eV, magenta). Reprinted with permission from ref. [23], Copyright (2020) American Chemical Society.

From the relative abundances of sp^2 C–C bonds and sp^3 C–C bonds in Table 3.4, the sp^2/sp^3 ratio can be calculated (Table 3.5), which is generally in accordance with the I_G/I_{Diamond} results estimated from Raman spectroscopy.

Table 3.5 sp^2/sp^3 ratio of BDD electrodes measured by XPS.

	sp^2/sp^3
0.1% no- sp^2	0.00
0.1% mid- sp^2	0.12
0.1% high- sp^2	5.25
1% no- sp^2	0.00
1% mid- sp^2	0.01
1% high- sp^2	0.02

The relative abundance of C–O bonds increases with increasing amounts of sp^2 in the 0.1% BDD electrodes, while it is almost constant for the 1% BDD electrodes. The large amount of surface oxygen on the 0.1% BDD electrodes containing sp^2 is considered to inhibit electron transfer by blocking electrochemically active sites [35]. Since inner-sphere electron transfer is surface sensitive, the changing electrochemical performance in $Fe(CN)_6^{4-/3-}$ and $Fe^{2+/3+}$, shown in Fig. 3.6b and Fig. 3.6c, can be ascribed to the increased abundance of C–O bonds. Moreover, the distribution of functional group on the surface significantly influences the value of the work function by interfacial dipole alignment [36,37]. UPS spectra (Fig. 3.8 and Table 3.6) revealed that the work function Φ increases with the sp^2 content of the 0.1% BDD electrodes, which is consistent with the increased C–O abundance in the XPS results.

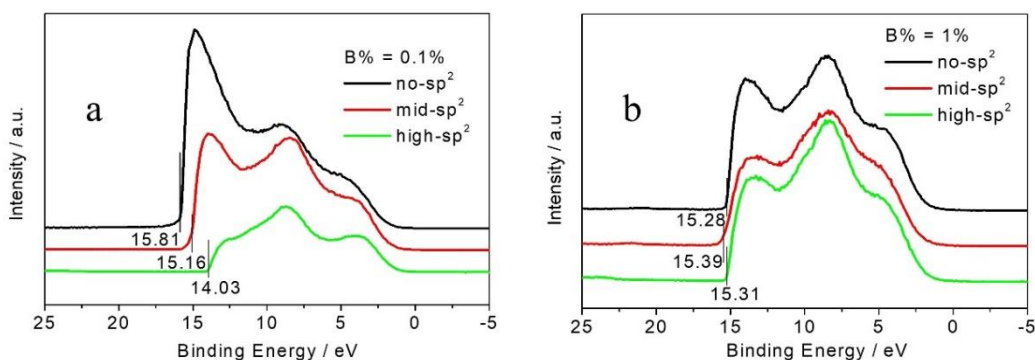


Fig. 3.8 UPS spectra of 0.1% BDDs (a), 1% BDDs (b). The cutoff position of each sample was located at the highest binding energy. Reprinted with permission from ref. [23], Copyright (2020) American Chemical Society.

Table 3.6 Band energies of BDDs deduced from UPS measurement

	B% = 0.1 %			B% = 1 %		
	no-sp ²	mid-sp ²	high-sp ²	no-sp ²	mid-sp ²	high-sp ²
cutoff	15.81	15.16	14.03	15.28	15.39	15.31
Φ	5.39	6.04	7.17	5.92	5.81	5.89

In Fig. 3.8, binding energy (BE) 0 eV was referred to the simultaneously measured Au plate. Work function (Φ) of each BDD shown in Table 3.6 is numerically equal to $21.2 - BE_{\text{highest}}$ (cutoff). The work function of Au (not shown) based on this definition was estimated to be 5.1 eV, which was in good agreement with literature [38].

On the other hand, electron transfer of outer-sphere redox species is insensitive to the surface morphology or termination but strongly influenced by carrier density. The sp² species on the surface probably act as trapping

centers which decrease the carrier density of the BDD [9,39], making the electron transfer rate rather slow. Mott–Schottky plots (Fig. 3.9 and Table 3.7) provide evidence of reduced carrier density with increasing amounts of sp² on 0.1% BDD electrodes. The calculation conditions are described as following. The CV performance in Ru(NH₃)₆^{3+/2+}, shown in Fig. 3.6a, can be interpreted on the basis of the decreasing carrier density.

The Mott–Schottky plot for each BDD electrode (Fig. 3.9) shows a negative slope which indicates that the materials are all p-type semiconductors [40,41]. The Mott–Schottky relation for a p-type semiconducting material is given by:

$$\frac{1}{C^2} = \frac{2}{\varepsilon\varepsilon_0 A^2 eN} \left(E - E_{fb} + \frac{kT}{e} \right) \quad (3)$$

where, C is the depletion layer capacitance, ε is the relative permittivity of the medium, ε_0 is the free space permittivity, A is the area of the electrode, e is the charge of an electron, N is the carrier density, E is the applied potential, E_{fb} is the flat band potential, k is the Boltzmann constant and T is the absolute temperature. At room temperature, the value of kT/e is approximated as zero. The carrier density can be calculated from the slope of the Mott-Schottky plot. The value of the flat band potential is estimated by extrapolation of the Mott–Schottky plot to the x-axis to find the intercept, which are summarized in Table 3.7.

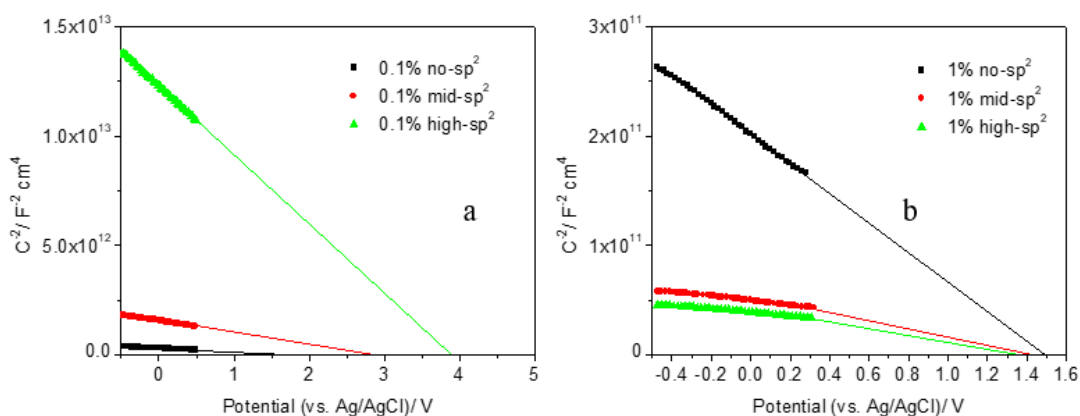


Fig. 3.9 Mott-Schottky plots of (a) 0.1% BDD samples and (b) 1% BDD samples containing various amounts of sp^2 . Electrolyte: 0.1 M H_2SO_4 ; frequency: 5000 Hz. Reprinted with permission from ref. [23], Copyright (2020) American Chemical Society.

Table 3.7 Carrier density and flat band potential of BDD samples by Mott-Schottky plot measurement.

	0.1%			1%		
	no- sp^2	mid- sp^2	high- sp^2	no- sp^2	mid- sp^2	high- sp^2
$N(\text{cm}^{-3})$	1.45 $\times 10^{20}$	4.55 $\times 10^{19}$	7.61 $\times 10^{18}$	1.95 $\times 10^{20}$	4.79 $\times 10^{20}$	5.16 $\times 10^{20}$
$E_{fb}(\text{V})$	1.73	2.84	4.06	1.47	1.43	1.36

In contrast to the abundance of C–O bonds, the abundance of sp^3 C–C bonds decreases dramatically with increasing sp^2 content on the 0.1% BDD electrodes. The phenomenon of decreasing sp^3 C–C bonds is apparent in the graphitization process of diamond [42], in which both disordered carbon (amorphous carbon) and graphitic phase components are found. It is

surmised that the sp^3 C–C bonds in the 0.1% high- sp^2 sample are partially converted to amorphous carbon.

From the above results we conclude that the large difference in surface oxygen is the main reason for the different inner-sphere electron transfer rates, which is proven by XPS/UPS analysis, whereas the various carrier densities lead to the different electron transfer behavior in the outer-sphere pathway, which is supported by the Mott–Schottky plot results.

3.4 Conclusion

In contrast to the general behavior observed for the effect of sp^2 on normal BDD, low-boron-doped BDD displayed less active electrochemical behavior with increasing sp^2 content. Wider potential windows and lower electron transfer rates for both inner-sphere and outer-sphere redox reactions were found with low-boron-doped BDD containing sp^2 than with low-boron-doped BDD without sp^2 , which is opposite from the results found with normal BDD. The unusual electron transfer properties were well interpreted by analysis of the surfaces of the BDD samples by XPS, UPS, and the carrier density by Mott–Schottky plots. The distinctive behavior of low-boron-doped diamond electrodes containing sp^2 carbon is induced by multiple factors, including the greater abundance of surface oxygen, the increased work function, the reduced carrier density, and the existence of amorphous carbon.

3.5 References

- [1] T. Watanabe, Y. Honda, K. Kanda, Y. Einaga, Tailored design of boron-doped diamond electrodes for various electrochemical applications with boron-doping level and sp^2 -bonded carbon impurities, *Phys. Status Solidi*. 211 (2014) 2709–2717.

- [2] T. Kashiwada, T. Watanabe, Y. Ootani, Y. Tateyama, Y. Einaga, A Study on Electrolytic Corrosion of Boron-Doped Diamond Electrodes when Decomposing Organic Compounds, *ACS Appl. Mater. Interfaces*. 8 (2016) 28299–28305.
- [3] Y. Einaga, J.S. Foord, G.M. Swain, Diamond electrodes: Diversity and maturity, *MRS Bull.* 39 (2014) 525–532.
- [4] K.K. Cline, M.T. McDermott, R.L. McCreery, Anomalously slow electron transfer at ordered graphite electrodes: Influence of electronic factors and reactive sites, *J. Phys. Chem.* 98 (1994) 5314–5319.
- [5] J.A. Bennett, J. Wang, Y. Show, G.M. Swain, Effect of sp^2 -Bonded Nondiamond Carbon Impurity on the Response of Boron-Doped Polycrystalline Diamond Thin-Film Electrodes, *J. Electrochem. Soc.* 151 (2004) E306-E311.
- [6] S. Garcia-Segura, E. Vieira Dos Santos, C.A. Martínez-Huitle, Role of sp^3/sp^2 ratio on the electrocatalytic properties of boron-doped diamond electrodes: A mini review, *Electrochem. Commun.* 59 (2015) 52–55.
- [7] J. V. Macpherson, *The Use of Conducting Diamond in Electrochemistry*, 2016.
- [8] Z.J. Ayres, S.J. Cobb, M.E. Newton, J. V. Macpherson, Quinone electrochemistry for the comparative assessment of sp^2 surface content of boron doped diamond electrodes, *Electrochem. Commun.* 72 (2016) 59–63.
- [9] Z.J. Ayres, A.J. Borrill, J.C. Newland, M.E. Newton, J. V. Macpherson, Controlled sp^2 Functionalization of Boron Doped Diamond as a Route for the Fabrication of Robust and Nernstian pH Electrodes, *Anal. Chem.* 88 (2016) 974–980.
- [10] R.E.P. Meyler, M.A. Edwards, J. V. Macpherson, Exploring the suitability of different electrode materials for hypochlorite quantification at high concentration in alkaline solutions, *Electrochem. Commun.* 86 (2018)

21–25.

[11] C.D.N. Brito, D.M. De Araújo, C.A. Martínez-Huitle, M.A. Rodrigo, Understanding active chlorine species production using boron doped diamond films with lower and higher sp^3/sp^2 ratio, *Electrochem. Commun.* 55 (2015) 34–38.

[12] T.L. Read, S.J. Cobb, J. V. Macpherson, An sp^2 Patterned Boron Doped Diamond Electrode for the Simultaneous Detection of Dissolved Oxygen and pH, *ACS Sensors.* 4 (2019) 756–763.

[13] S. Yu, N. Yang, M. Vogel, S. Mandal, O.A. Williams, S. Jiang, H. Schönherr, B. Yang, X. Jiang, Battery-like Supercapacitors from Vertically Aligned Carbon Nanofiber Coated Diamond: Design and Demonstrator, *Adv. Energy Mater.* 8 (2018) 1–10.

[14] K. Takagi, K. Natsui, T. Watanabe, Y. Einaga, Increasing the Electric Double-Layer Capacitance in Boron-Doped Diamond Electrodes, *ChemElectroChem.* 6 (2019) 1683–1687.

[15] A. Fujishima, Y. Einaga, T.N. Rao, D.A. Tryk, *Diamond Electrochemistry*, Elsevier B.V., Tokyo, 2005.

[16] J. V. Macpherson, The Use of Conducting Diamond in Electrochemistry, in: *Electrochem. Carbon Electrodes*, Wiley-VCH Verlag GmbH & Co. KGaA, 2016.

[17] J.P. Lagrange, A. Deneuve, E. Gheeraert, Activation energy in low compensated homoepitaxial boron-doped diamond films, *Diam. Relat. Mater.* 7 (1998) 1390–1393.

[18] K. Natsui, H. Iwakawa, N. Ikemiya, K. Nakata, Y. Einaga, Stable and Highly Efficient Electrochemical Production of Formic Acid from Carbon Dioxide Using Diamond Electrodes, *Angew. Chemie Int. Ed.* 57 (2018) 2639–2643.

[19] J. Xu, K. Natsui, S. Naoi, K. Nakata, Y. Einaga, Effect of doping level

on the electrochemical reduction of CO₂ on boron-doped diamond electrodes, *Diam. Relat. Mater.* 86 (2018) 167–172.

[20] M. Brycht, K. Kaczmarek, B. Uslu, S.A. Ozkan, S. Skrzypek, Sensitive determination of anticancer drug imatinib in spiked human urine samples by differential pulse voltammetry on anodically pretreated boron-doped diamond electrode, *Diam. Relat. Mater.* 68 (2016) 13–22.

[21] S. Pysarevska, L. Dubenska, S. Plotycya, E. Švorc, A state-of-the-art approach for facile and reliable determination of benzocaine in pharmaceuticals and biological samples based on the use of miniaturized boron-doped diamond electrochemical sensor, *Sensors Actuators, B Chem.* 270 (2018) 9–17.

[22] Z.J. Ayres, J.C. Newland, M.E. Newton, S. Mandal, O.A. Williams, J. V. Macpherson, Impact of chemical vapour deposition plasma inhomogeneity on the spatial variation of sp² carbon in boron doped diamond electrodes, *Carbon.* 121 (2017) 434–442.

[23] J. Xu, Y. Yokota, R.A. Wong, Y. Kim, Y. Einaga, Unusual Electrochemical Properties of Low-Doped Boron-Doped Diamond Electrodes Containing sp² Carbon, *J. Am. Chem. Soc.*, 2020, 142, 2310-2316.

[24] T. Watanabe, S. Yoshioka, T. Yamamoto, H. Sephiri-Amin, T. Ohkubo, S. Matsumura, Y. Einaga, The local structure in heavily boron-doped diamond and the effect this has on its electrochemical properties, *Carbon.* 137 (2018) 333–342.

[25] T. Watanabe, T.K. Shimizu, Y. Tateyama, Y. Kim, M. Kawai, Y. Einaga, Giant electric double-layer capacitance of heavily boron-doped diamond electrode, *Diam. Relat. Mater.* 19 (2010) 772–777.

[26] V. Mortet, Z. Vlčková Živcová, A. Taylor, O. Frank, P. Hubík, D. Trémouilles, F. Jomard, J. Barjon, L. Kavan, Insight into boron-doped diamond Raman spectra characteristic features, *Carbon.* 115 (2017) 279–284.

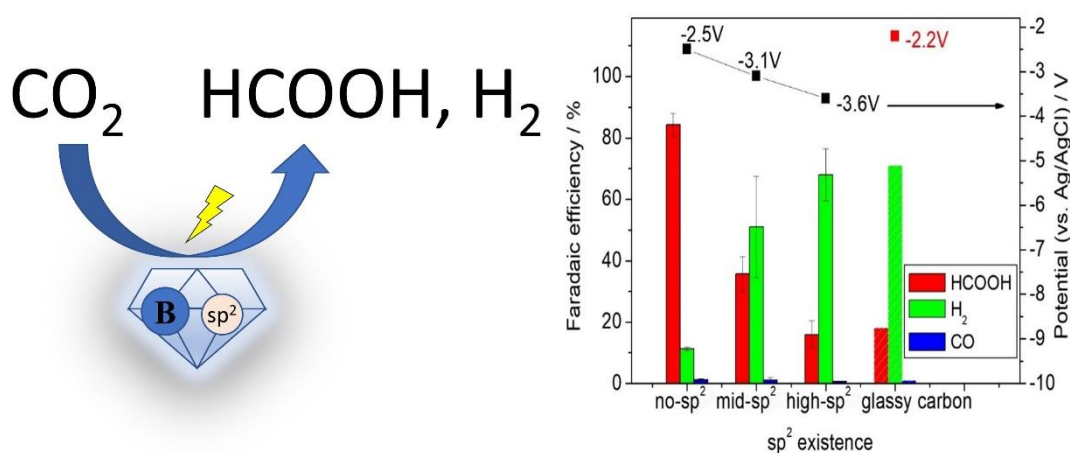
- [27] A.C. Ferrari, J. Robertson, Raman spectroscopy of amorphous, nanostructured, diamond-like carbon, and nanodiamond, *Philos. Trans. R. Soc. A Math. Phys. Eng. Sci.* 362 (2004) 2477–2512.
- [28] M.C. Granger, M. Witek, J. Xu, J. Wang, M. Hupert, A. Hanks, M.D. Koppang, J.E. Butler, G. Lucazeau, M. Mermoux, J.W. Strojek, G.M. Swain, Standard Electrochemical Behavior of High-Quality, Boron-Doped Polycrystalline Diamond Thin-Film Electrodes, *Anal. Chem.* 72 (2000) 3793–3804.
- [29] A.C. Ferrari, J. Robertson, Resonant Raman spectroscopy of disordered, amorphous, and diamondlike carbon, *Phys. Rev. B.* 64 (2001) 075414.
- [30] N.R. Wilson, S.L. Clewes, M.E. Newton, P.R. Unwin, J. V. Macpherson, Impact of grain-dependent boron uptake on the electrochemical and electrical properties of polycrystalline boron doped diamond electrodes, *J. Phys. Chem. B.* 110 (2006) 5639–5646.
- [31] P. Chen, R.L. McCreery, Control of Electron Transfer Kinetics at Glassy Carbon Electrodes by Specific Surface Modification, *Anal. Chem.* 68 (1996) 3958–3965.
- [32] Lavagnini, I.; Antiochia, R.; Magno, F. An Extended Method for the Practical Evaluation of the Standard Rate Constant from Cyclic Voltammetric Data. *Electroanalysis* 2004, 16 (6), 505–506.
- [33] Nicholson, R. S. Theory and Application of Cyclic Voltammetry for Measurement of Electrode Reaction Kinetics. *Anal. Chem.* 1965, 37 (11), 1351–1355.
- [34] Patten, H. V.; Meadows, K. E.; Hutton, L. A.; Iacobini, J. G.; Battistel, D.; McKelvey, K.; Colburn, A. W.; Newton, M. E.; MacPherson, J. V.; Unwin, P. R. Electrochemical Mapping Reveals Direct Correlation between Heterogeneous Electron-Transfer Kinetics and Local Density of States in Diamond Electrodes. *Angew. Chemie - Int. Ed.* 2012, 51 (28), 7002–7006.

- [35] L.A. Hutton, J.G. Iacobini, E. Bitziou, R.B. Channon, M.E. Newton, J. V. Macpherson, Examination of the factors affecting the electrochemical performance of oxygen-terminated polycrystalline boron-doped diamond electrodes, *Anal. Chem.* 85 (2013) 7230–7240.
- [36] D.M. Alloway, M. Hofmann, D.L. Smith, N.E. Gruhn, A.L. Graham, R. Colorado, V.H. Wysocki, T.R. Lee, P.A. Lee, N.R. Armstrong, Interface Dipoles Arising from Self-Assembled Monolayers on Gold: UV-Photoemission Studies of Alkanethiols and Partially Fluorinated Alkanethiols, *J. Phys. Chem. B.* 107 (2003) 11690–11699.
- [37] H. Ishii, K. Sugiyama, E. Ito, K. Seki, Energy Level Alignment and Interfacial Electronic Structures at Organic/Metal and Organic/Organic Interfaces, *Adv. Mater.* 11 (1999) 605–625.
- [38] Chun, W. J.; Ishikawa, A.; Fujisawa, H.; Takata, T.; Kondo, J. N.; Hara, M.; Kawai, M.; Matsumoto, Y.; Domen, K. Conduction and Valence Band Positions of Ta₂O₅, TaON, and Ta₃N₅ by UPS and Electrochemical Methods. *J. Phys. Chem. B* 2003, 107 (8), 1798–1803.
- [39] S.R.P. Silva, B. Rafferty, G.A.J. Amaratunga, J. Schwan, D.F. Franceschini, L.M. Brown, Nitrogenated amorphous carbon as a semiconductor, *Diam. Relat. Mater.* 5 (1996) 401–404.
- [40] Rao, T. N.; Tryk, D. A.; Hashimoto, K.; Fujishima, A. Band-Edge Movements of Semiconducting Diamond in Aqueous Electrolyte Induced by Anodic Surface Treatment. *J. Electrochem. Soc.* 1999, 146 (2), 680–684.
- [41] Alehashem, S.; Chambers, F.; Strojek, J. W.; Swain, G. M.; Ramesham, R. Cyclic Voltammetric Studies of Charge Transfer Reactions at Highly Boron-Doped Polycrystalline Diamond Thin-Film Electrodes. *Anal. Chem.* 1995, 67 (17), 2812–2821.
- [42] O. Romanyuk, M. Varga, S. Tulic, T. Izak, P. Jiricek, A. Kromka, V. Skakalova, B. Rezek, Study of Ni-Catalyzed Graphitization Process of Diamond by in Situ X-ray Photoelectron Spectroscopy, *J. Phys. Chem. C.*

122 (2018) 6629–6636.

Chapter 4

Effect of sp^2 species in a boron-doped diamond electrode on the electrochemical reduction of CO_2



Reproduced from Xu, J.; Einaga, Y., *Electrochem. Comm.*, **2020**, 115, 106731-106734. with permission from Elsevier.

4.1 Introduction

As described in previous chapter, the presence of sp^2 carbon has a direct effect on the band structure and the density of state (DOS), and have a strong influence on the electrochemical properties [85]. BDDs containing sp^2 carbon are normally considered to be of low quality, since they have a greater background current [43] and are easier to corrode [86] than material with no sp^2 carbon. Nevertheless, sp^2 -containing BDD has performed very well in a number of applications, including the treatment of waste water [87], oxygen reduction [88], and the generation of ozone [43]. The products of CO_2 reduction on BDD without sp^2 carbon are mainly $HCOOH$ [73]. However, CO_2 reduction using sp^2 carbon electrodes such as glassy carbon (GC), graphite, graphene and HOPG have shown a tendency for CO to be the main product [89–92]. This difference in the products of CO_2RR has been reported to be related to the adsorbability of the electrode surface [26].

In this chapter, we have studied the electrochemical reduction of CO_2 on BDD electrodes with various sp^2/sp^3 ratios, which were identified by Raman spectroscopy [93]. BDD containing 0.1% boron was selected as a candidate for further investigation owing to its excellent performance in CO_2 reduction compared to BDD electrodes with other B/C ratios [94]. This study should help in elucidating the electrocatalytic properties of the BDD electrode towards the CO_2RR .

4.2 Experimental

4.2.1 Preparation of BDD working electrode

BDDs with different carbon sp^2 levels were fabricated by MPCVD (AX6500X, CORNES Technologies corp.). By modifying the gas flow rates of the boron source $B(CH_3)_3$, the carbon source CH_4 and the carrier gas H_2 , BDDs with a boron to carbon ratio (B/C) of 0.1% and a variety of sp^2/sp^3 ratios were deposited on silicon wafers as described elsewhere [93].

Commercial GC electrodes (Tokai Corp.) were used for comparison, and were smoothed by grinding before use.

The surface morphology was observed by SEM (JCM-6000, JEOL). Raman spectra were recorded with an excitation wavelength of 532 nm in ambient air at room temperature with an Acton SP2500 (Princeton Instruments). The sp^2/sp^3 ratios (I_G/I_{Diamond}) estimated from the Raman data are listed in Table 4.1. The samples were defined as no- sp^2 , mid- sp^2 and high- sp^2 (details of this assignment are given in [93]). The actual boron content of each BDD was estimated by Glow Discharge Optical Emission Spectroscopy (GDOES) (GD-Profilier2, Horiba Ltd.) with reference to a BDD sample whose boron content had already been estimated by SIMS [43].

Table 4.1 B/C ratio and I_G/I_{Diamond} values of BDDs used in Fig. 4.4

B/C ratio (%)	I_G/I_{Diamond}		
	no- sp^2	mid- sp^2	high- sp^2
0.03	0	0.02	0.03
0.07	0	0.09	0.11
0.15	0	0.05	0.1
0.70	0	0.04	0.15
2.20	0	0.08	0.09

4.2.2 Electrochemical reduction of CO_2

The electrochemical measurements were conducted in a two-compartment flow cell separated with a Nafion membrane (NRE-212, 0.002 in thickness, Aldrich), as described in our previous research [73,94]. The fabricated BDD, Pt plate and Ag/AgCl (in saturated KCl) were used as the working electrode, counter electrode and reference electrode, respectively. The geometric areas of both the BDD and Pt electrode in contact with the electrolyte were 9.62 cm^2 . Prior to every electrochemical measurement, two steps of electrochemical pretreatment using cyclic voltammetry (CV) in 0.1

M H₂SO₄ aqueous solution were conducted to ensure that the surface termination was consistent. The first step was performed from -3.5 V to +3.5 V (vs. Ag/AgCl) for 10 cycles at a scan rate of 1 V s⁻¹. The second step was performed from 0 V to +3.5 V (vs. Ag/AgCl) for 20 cycles at 1 V s⁻¹. Fundamental electrochemical properties such as the potential window and the CV performed in redox electrolytes were as shown in other reports [93].

The electrochemical reduction of CO₂ was performed using the following procedure. The catholyte and anolyte were aqueous solutions of 0.5 M KCl and 1 M KOH, respectively. Both catholyte and anolyte were 50 mL solutions and were circulated separately in the cell with a flow rate of 100 mL min⁻¹ by means of separate pumps. The catholyte was purged with N₂ gas for 30 min at 200 sccm to remove any dissolved oxygen and then bubbled with CO₂ gas for 1 hour at 500 sccm to saturate it with CO₂. After N₂ and CO₂ saturation, linear sweep voltammetry (LSV) measurements were carried out in the potential range from 0 V to -4 V (vs. Ag/AgCl) at 0.02 V s⁻¹. The chronopotentiometry reductions were performed under a constant current density of -2 mA cm⁻² for 1 hour. The chronoamperometry reductions were at -2.2 V, -2.5 V, -2.7 V, -2.9 V and -3.4 V (vs. Ag/AgCl) for 1 hour. During the reduction, CO₂ was continually bubbled into the catholyte at a slow flow rate. After the electrolysis, N₂ gas was bubbled into the catholyte for 15 min at 50 sccm and the gaseous products collected in an aluminum bag (CEK 3008-26401, GL Science). The products were analyzed by gas chromatography and high-performance liquid chromatography (HPLC). The quantity of H₂ and the CO content were measured by gas chromatography (GC-2014, Shimadzu Corp.) with a thermal conductivity detector and flame ionization detector. The formic acid concentration was quantified by HPLC with an electroconductivity detector (Prominence, Shimadzu Corp.). The Faradaic efficiency was estimated from the yield of each product, as described elsewhere [73].

4.3 Results and discussion

4.3.1 Characterization of the BDDs

Basic characterization results for the samples, such as the actual B/C ratio, I_G / I_{Diamond} and the average grain size have been reported in a previous study [93]. It is important to emphasise that the actual B/C ratios of the three BDDs studied (0.08%, 0.06% and 0.07%) are roughly equal to each other, and therefore any drastic change in electrochemical reduction could not be due to a difference in the boron content of the electrodes. The I_G / I_{Diamond} ratios (0, 0.09 and 0.11) were obtained by Raman analysis. Each sample revealed a clear first-order diamond peak at 1332 cm^{-1} . A broad band around 1550 cm^{-1} was found in the spectra of mid- sp^2 and high- sp^2 BDD, which confirms the presence of sp^2 sites (amorphous carbon and graphitic carbon). By contrast, the no- sp^2 BDD showed a negligible level of sp^2 defects. Furthermore, using SEM, the average grain size of the BDDs (13.0, 10.6 and $9.5 \mu\text{m}$) was found to decrease with increasing sp^2 content. Additionally, there are more boundaries on sp^2 -containing BDD [53,95] and a greater proportion of (111) facets than in the sp^2 -free diamonds. This indicates that secondary nucleation is extended by enhancing the sp^2 character [85].

4.3.2 CO_2 reduction on sp^2 -containing BDD

LSV before and after CO_2 bubbling

The electrocatalytic activity of the BDDs was examined in CO_2 -saturated 0.5 M KCl solutions. The LSV curves before and after CO_2 bubbling are shown in Fig. 4.1, in which the potential was swept between -1 V and -3.5 V (vs. Ag/AgCl) at a rate of 0.02 V s^{-1} .

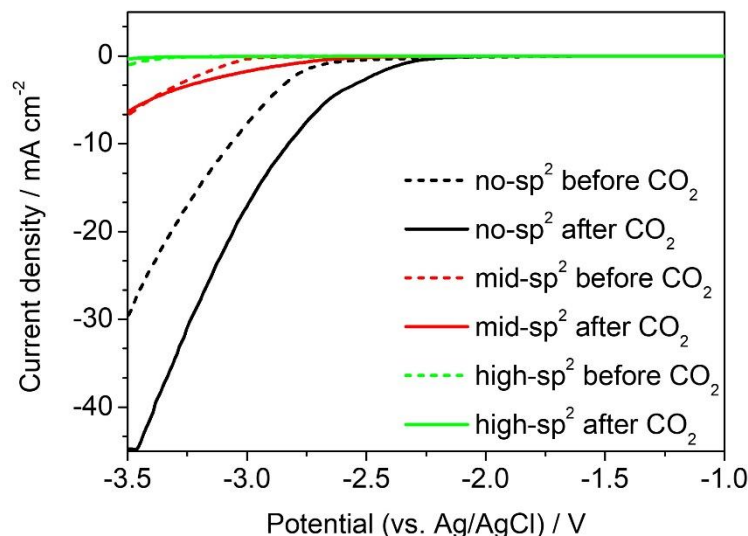


Fig. 4.1 Electrochemical performance of different electrodes by mean of an LSV scan with a scan rate of 0.02 V s^{-1} in 0.5 M KCl aqueous electrolyte before and after CO_2 saturation. Reproduced from ref. [16], copyright (2020), with permission from Elsevier.

Comparing the LSVs with increasing sp^2 content after CO_2 bubbling in Fig. 4.1 (solid lines), two clear changes in the voltammograms are noticeable. There is an obvious negative shift of the onset potential from -2.3 V to -2.6 V and -3.4 V (vs. Ag/AgCl) with increasing sp^2 content. On the other hand, a sizeable decrease in the anodic current at -3.5 V was observed from approximately 45 mA cm^{-2} to 7 mA cm^{-2} and 1 mA cm^{-2} in samples with increasing sp^2 content. The measured current was composed of two parts: a partial current from HER and partial current from CO_2RR . One possible reason for the negative shift in the potential and decreased current is the diminished carrier density caused by the increasing sp^2/sp^3 ratio [93], which also inhibits the CO_2RR activity.

Reduction with constant current density

Fig. 4.2 shows the products of CO₂ reduction and the corresponding reduction potentials on various BDD electrodes and also on a GC electrode. The results were obtained at constant current density of -2 mA cm^{-2} for 1 hour. It can be seen that the tendency towards HCOOH production decreases with increasing sp² content, while the tendency towards H₂ production increased. The results show the reduction potential shifting to more negative values with increasing sp² content. The reduction potential decreased from -2.5 V to -3.1 V and -3.6 V (vs. Ag/AgCl) for no-sp², mid-sp² and high-sp² electrodes, respectively, which to some extent agrees with the LSV results in Fig. 4.1.

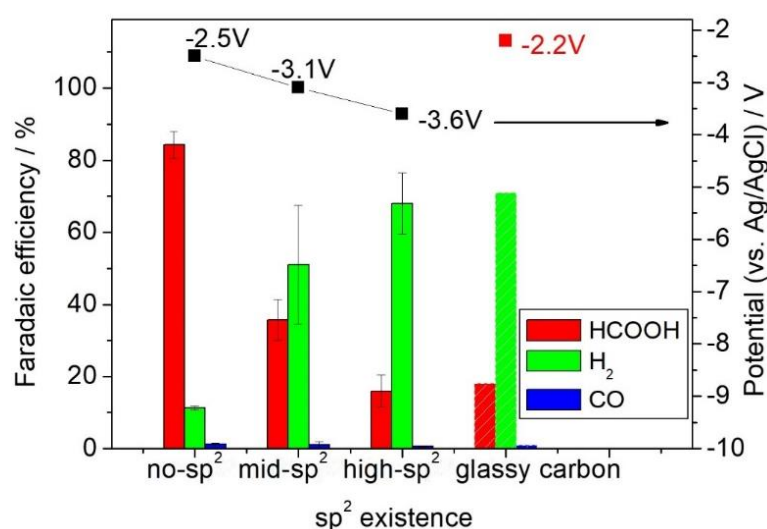


Fig. 4.2 Faradaic efficiency of CO₂RR on different electrodes and the corresponding potential, under a constant current density of -2 mA cm^{-2} for a 1 h reduction. Reproduced from ref. [16], copyright (2020), with permission from Elsevier.

As indicated by previous studies, HCOOH is the main product of the electrochemical reduction of CO₂ by BDD electrodes with a low sp² content [73,94]. This is also shown by the data for no-sp² BDD in Fig. 4.2, for which

the Faradaic efficiency was as high as 84% for HCOOH. The performance of mid-sp² BDDs, at 36% efficiency for producing HCOOH, was not as high as for the no-sp² BDD electrode. Rather like GC electrodes, which contain sp² over the entire surface and have 18% efficiency for HCOOH, high-sp² BDD had a 16% HCOOH efficiency. However, H₂ evolution increased with increasing sp² content, with efficiency values of 11% for no-sp² BDD, 51% for mid-sp² BDD, 68% for high-sp² BDD and 71% for GC, respectively. These results suggest that the amount of sp² carbon present has a significant influence on the selectivity of the CO₂RR [96].

Potential dependence

Fig. 4.3 shows the dependence of the Faradaic efficiency on the electrode potential from -4 V to -2.2 V (vs. Ag/AgCl) for each electrode. With increasing sp² content, the optimized potential for maximum production of HCOOH moves to a more negative potential. Furthermore, the maximum Faradaic efficiency value for producing HCOOH decreases. As can be seen in Fig. 4.3(a), the highest Faradaic efficiencies for HCOOH for no-sp², mid-sp² and high-sp² electrodes were obtained at constant potentials of -2.5 V, -2.9 V and -3.4 V (vs. Ag/AgCl), respectively. These values are in accordance with the onset potentials measured by the LSV curves in Fig. 4.1. The Faradaic efficiencies were correspondingly reduced to 78%, 62% and 12%, respectively.

The minimum Faradaic efficiency for H₂ also revealed a negative potential shift. The no-sp² BDD sample produced the least H₂ at -2.5 V (vs. Ag/AgCl), and the high-sp² and mid-sp² were at -2.7 V and -2.9 V (vs. Ag/AgCl), respectively.

The Faradaic efficiency for production of CO on all electrodes was lower than 10%. However, the high-sp² BDD produced more CO than the other BDDs in the potential range from -3.4 V to -2.5 V (vs. Ag/AgCl). The highest Faradaic efficiency of high-sp² BDD is 7% at a potential of -2.9 V

(vs. Ag/AgCl). The results indicate that a CO₂RR producing CO is easier to obtain on BDDs containing sp² species than on BDDs with no sp² carbon.

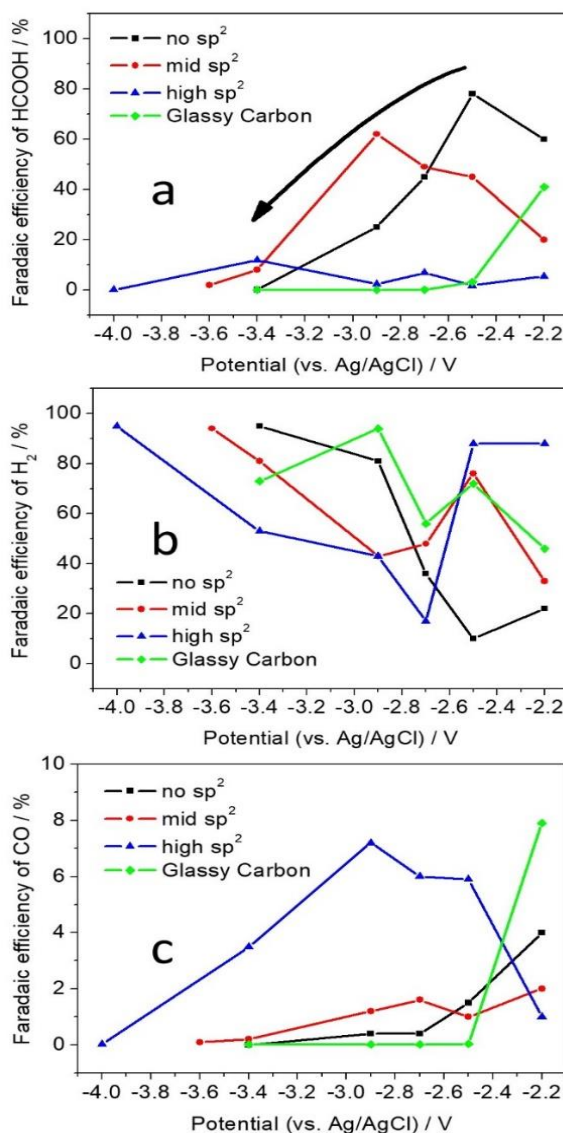


Fig. 4.3 Faradaic efficiency of generating (a) HCOOH, (b) H₂ and (c) CO on different electrodes under a constant potential from -3.4 V to -2.2 V (vs. Ag/AgCl) respectively. Reproduced from ref. [16], copyright (2020), with permission from Elsevier.

4.3.3 Proposed mechanism

The presence of sp^2 carbon clearly affects the rate of reduction of CO_2 under constant current, which is a competition between CO_2RR and HER. For BDD electrodes in the absence of sp^2 carbon, HCOOH is the major product, whilst H_2 is a minor product. Our results indicate that CO_2RR performs much better than HER on a sp^3 surface. This phenomenon is ascribed to the wide potential window of BDD, allowing the HER to be minimized and CO_2RR to become the main reaction [73]. The yield of H_2 is changed a great deal on varying the applied potential, which indicates that the HER on this electrode is sensitive to potential. By contrast, the BDD electrodes containing sp^2 species produced more H_2 than HCOOH. This distribution of products is probably affected by the adsorption sites present on sp^2 carbon [97].

The products of CO_2RR are a mixture of HCOOH and CO. On BDD electrodes without sp^2 species, HCOOH was the main outcome and CO is a minor product. On the other hand, BDD electrodes containing sp^2 produce a smaller amount of HCOOH and a relatively higher amount of CO. It is suggested that the sp^2 surface has a higher adsorption of $CO_2^{\bullet-}$ and that this affects the products of the CO_2RR [26]. It has previously been suggested that CO is generated on adsorbing electrode surfaces whilst HCOOH is produced on surfaces that do not show adsorption [9, 31].

The sp^2 effect on the CO_2RR is found not only on the 0.1% BDDs, but also on other samples with different boron contents. Fig. 4.4 shows the Faradaic efficiency for the production of HCOOH on BDD electrodes with various sp^2 content and with different B/C ratios (as listed in Table 4.1). For each boron doping level, HCOOH production efficiency declined with increasing sp^2 content.

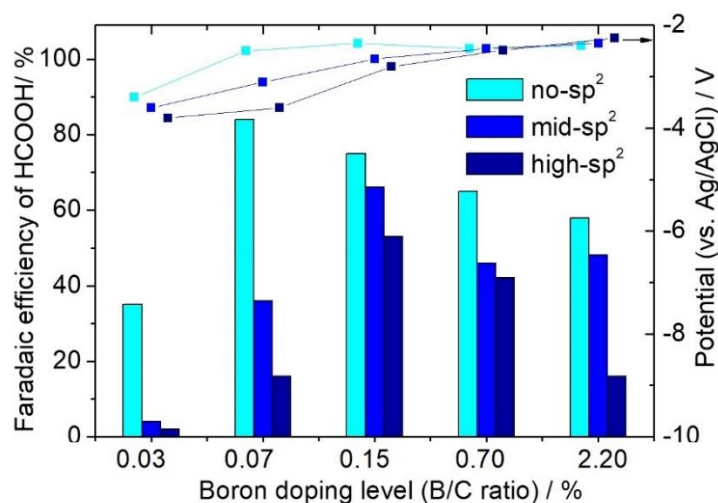


Fig. 4.4 Faradaic efficiency of HCOOH on electrodes with different boron doping/sp² content and the corresponding potentials under a constant current density of -2 mA cm^{-2} for a 1 h reduction. Reproduced from ref. [16], copyright (2020), with permission from Elsevier.

4.4 Conclusion

We have studied the influence of sp² carbon in BDD electrodes on the CO₂RR. BDDs with different sp²/sp³ ratios were produced by MPCVD and used as electrodes for the electrochemical reduction of CO₂. The products were found to demonstrate certain trends with increasing sp² content. We observed that there is a sharp decline in the production of HCOOH with increasing sp² content. On the other hand, the yield of H₂ was significantly raised. The results for BDD electrodes with high sp² content were similar to those of a well-known sp² electrode (GC). Moreover, our results revealed a negative shift in the onset potential for the reduction and a lower maximum yield of HCOOH with increasing sp² content. It is suggested that the surface of sp²-containing BDDs could adsorb CO₂^{•-} more easily than those without sp² species, although further investigation is required. It is noteworthy that the selectivity of CO₂ reduction could be controlled by adjusting the distribution of carbonaceous species within the BDD electrode.

4.5 References

- [1] J.A. Bennett, J. Wang, Y. Show, G.M. Swain, Effect of sp^2 -Bonded Nondiamond Carbon Impurity on the Response of Boron-Doped Polycrystalline Diamond Thin-Film Electrodes, *J. Electrochem. Soc.* 151 (2004) E306-E313.
- [2] T. Watanabe, Y. Honda, K. Kanda, Y. Einaga, Tailored design of boron-doped diamond electrodes for various electrochemical applications with boron-doping level and sp^2 -bonded carbon impurities, *Phys. Status Solidi.* 211 (2014) 2709–2717.
- [3] T. Kashiwada, T. Watanabe, Y. Ootani, Y. Tateyama, Y. Einaga, A Study on Electrolytic Corrosion of Boron-Doped Diamond Electrodes when Decomposing Organic Compounds, *ACS Appl. Mater. Interfaces.* 8 (2016) 28299–28305.
- [4] C.D.N. Brito, D.M. De Araújo, C.A. Martínez-Huitle, M.A. Rodrigo, Understanding active chlorine species production using boron doped diamond films with lower and higher sp^3/sp^2 ratio, *Electrochem. Commun.* 55 (2015) 34–38.
- [5] T.L. Read, S.J. Cobb, J. V. Macpherson, An sp^2 Patterned Boron Doped Diamond Electrode for the Simultaneous Detection of Dissolved Oxygen and pH, *ACS Sensors.* 4 (2019) 756–763.
- [6] K. Natsui, H. Iwakawa, N. Ikemiya, K. Nakata, Y. Einaga, Stable and Highly Efficient Electrochemical Production of Formic Acid from Carbon Dioxide Using Diamond Electrodes, *Angew. Chemie Int. Ed.* 57 (2018) 2639–2643.
- [7] K. Hara, A. Kudo, T. Sakata, Electrochemical CO_2 reduction on a glassy carbon electrode under high pressure, *J. Electroanal. Chem.* 421 (1997) 1–4.
- [8] N. Sreekanth, M.A. Nazrulla, T.V. Vineesh, K. Sailaja, K.L. Phani, Metal-free boron-doped graphene for selective electroreduction of carbon

dioxide to formic acid/formate, *Chem. Commun.* 51 (2015) 16061–16064.

[9] N. Yang, S.R. Waldvogel, X. Jiang, *Electrochemistry of Carbon Dioxide on Carbon Electrodes*, *ACS Appl. Mater. Interfaces.* 8 (2016) 28357–28371.

[10] P. Han, X. Yu, D. Yuan, M. Kuang, Y. Wang, A.M. Al-Enizi, G. Zheng, *Defective graphene for electrocatalytic CO₂ reduction*, *J. Colloid Interface Sci.* 534 (2019) 332–337.

[11] A. Goepfert, M. Czaun, J.-P. Jones, G.K. Surya Prakash, G.A. Olah, *Recycling of carbon dioxide to methanol and derived products- closing the loop*, *Chem. Soc. Rev.* 43 (2014) 7995–8048.

[12] J. Xu, Y. Yokota, R.A. Wong, Y. Kim, Y. Einaga, *Unusual Electrochemical Properties of Low-Doped Boron-Doped Diamond Electrodes Containing sp² Carbon*, *J. Am. Chem. Soc.* 142 (2020) 2310–2316.

[13] J. Xu, K. Natsui, S. Naoi, K. Nakata, Y. Einaga, *Effect of doping level on the electrochemical reduction of CO₂ on boron-doped diamond electrodes*, *Diam. Relat. Mater.* 86 (2018) 167–172.

[14] J. V. Macpherson, *A practical guide to using boron doped diamond in electrochemical research*, *Phys. Chem. Chem. Phys.* 17 (2015) 2935–2949.

[15] T. Watanabe, S. Yoshioka, T. Yamamoto, H. Sepehri-Amin, T. Ohkubo, S. Matsumura, Y. Einaga, *The local structure in heavily boron-doped diamond and the effect this has on its electrochemical properties*, *Carbon.* 137 (2018) 333–342.

[16] D. Medeiros De Araújo, P. Cañizares, C.A. Martínez-Huitle, M.A. Rodrigo, *Electrochemical conversion/combustion of a model organic pollutant on BDD anode: Role of sp³/sp² ratio*, *Electrochem. Commun.* 47 (2014) 37–40.

[17] S. Garcia-Segura, E. Vieira Dos Santos, C.A. Martínez-Huitle, *Role of sp³/sp² ratio on the electrocatalytic properties of boron-doped diamond*

electrodes: A mini review, *Electrochem. Commun.* 59 (2015) 52–55.

[18] Y. Hori, H. Wakebe, T. Tsukamoto, O. Koga, Electrocatalytic process of CO selectivity in electrochemical reduction of CO₂ at metal electrodes in aqueous media, *Electrochim. Acta.* 39 (1994) 1833–1839.

Chapter 5

Summary and Future Perspective

5.1 Summary

This thesis represented tailored design of BDD electrode for electrochemical reduction of CO₂, which also described the influence of intrinsic character of BDD electrode on electrochemical properties. The intrinsic parameters of BDD, especially boron doping level and sp² impurity content, are optimized for better selectivity in electrochemical reduction of CO₂.

In Chapter 2, the relationship between boron content of BDD electrodes and the products of CO₂ reduction was presented. BDDs with various boron content (0.01%, 0.1%, 0.5%, 1%, 2%) were manufactured by MPCVD. Structural characterization, electrochemical characterization and electrochemical reduction of CO₂ were conducted. According to the above processes, we came up with the conclusion, that products of CO₂ reduction (HCOOH and CO) are affected by boron content. This research is important for design and control the electrode of electrochemical reduction of CO₂. Furthermore, it provides a relatively new way of improving selectivity of CO₂ reduction.

In Chapter 3, unusual sp²-related electrochemical properties of low boron-doped BDD were reported. They are in total contrast to those found with heavy or normally doped BDD, in which narrower potential windows and increased redox reactions are found with increasing amounts sp². The potential window of low-doped BDD with high sp² levels is as wide as 5.19 V in 0.1 M H₂SO₄ aq. solution, which is much larger than the 3~4 V for normally doped BDD reported in previous publications. The voltammograms for the redox reaction using this electrode are irreversible and without an anodic peak due to the slow kinetics. The unusual electron transfer properties were interpreted by analyzing the surface of the BDD samples by XPS, UPS and Mott-Schottky plots. The results of these analyses indicate that the distinctive behavior of low boron-doped diamond electrodes containing sp² carbon is induced by multiple factors, including the greater abundance of surface oxygen, the increased work function, the reduced

carrier density and the existence of amorphous carbon. Furthermore, this work provides a guideline for screening BDD electrodes for specific electrochemical applications.

In Chapter 4, the effect of sp^2 carbon within a BDD electrode on the electrochemical reduction of CO_2 has been investigated for the first time. As a result, with increasing sp^2 content, the faradaic efficiency for the production of H_2 were increased but that of $HCOOH$ was reduced. Moreover, the favorable electrolysis conditions for producing $HCOOH$ shifted towards the negative potential direction with increasing sp^2 content. This phenomenon was ascribed to the adsorption sites on the sp^2 carbon. This study will help elucidating the electrocatalytic properties of BDD electrode in the CO_2 reduction reaction.

5.2 Future perspective

It can be concluded that, BDD electrode is a promising ideal electrode material for electrochemical reduction of CO_2 , which showed relatively good selectivity of $HCOOH$ and CO under specified conditions. Nevertheless, it is still some problems existing.

5.2.1 For industrial application

For fulfilling the purpose of industrial application, large surface BDD films with high quality should be manufactured. At present, BDDs made by MPCVD is limited, due to size of plasma-generate chamber. Even though homogenous BDD surface is obtained ascribed to homogenous plasma, it is a deficiency for practical using of BDD in industry. To overcome it, other fabrication method like Hot-Filament CVD (HFCVD) process has been investigated to achieve large size BDD electrode for industrial application. With increasing filament, HFCVD could fabricate BDD with larger size.

Whereas durability of HFCVD-BDD is still not satisfied and the performance of CO₂ reduction is not stable. This is may be caused by the inhomogeneous surface which is affected by aging of tungsten filament in HFCVD. Therefore, further study of manufacturing and surface investigation of HFCVD-BDD is necessary in the future.

The other strategy for fulfilling industrial application is setting-up proper mass transfer system for large yield of production. So far, gas diffusion cell or flow cell has been used to improve mass transfer and achieve better production. Therefore, some effort on improving mass transfer should be made in the future.

5.2.2 Mechanism elucidation

More clearly understanding the mechanism of CO₂ reduction on BDD helps realizing tailor design more precisely.

Even though many experimental studies of CO₂ reduction (including production quantification and in-situ Infrared Spectra) indicated the conversion mechanism on BDD, theoretical study is still inadequate. Density functional theory (DFT) modelling process would be a convictive method for theoretical explanation of CO₂ reduction mechanism on BDD electrode.

Nevertheless, the investigation of intrinsic construction of BDD electrode on CO₂ reduction is to some extent insufficient. Beside boron doping level and sp² carbon impurity, the intrinsic construction research of BDD electrode would also including facet distribution, electrochemical active surface area, multiple heteroatoms doping and so on. Since the durability of BDD is based on the diamond structure, intrinsic construction changing may influence the service life, which should be noticed in the future study.

5.2.3 Other application of specific BDD

Excepting for the application of CO₂ reduction, BDD electrode introduced in Chapter 3 should be further investigated. The high sp² contained low-doped BDD may be used in the application of biological compound detection by taking advantage of its wide potential window and high surface oxygen.

List of Publications and Conferences

Published papers presented in this thesis:

(1) J. Xu, Y. Einaga,

“Effect of sp^2 species in a boron-doped diamond electrode on the electrochemical reduction of CO_2 ”,

Electrochemistry Communications, 115 (2020) 106731-106734.

(2) J. Xu, Y. Yokota, R.A. Wong, Y. Kim, Y. Einaga,

“Unusual Electrochemical Properties of Low-Doped Boron-Doped Diamond Electrodes Containing sp^2 Carbon”,

Journal of the American Chemical Society, 142 (2020) 2310–2316.

(3) J. Xu, K. Natsui, S. Naoi, K. Nakata, Y. Einaga,

“Effect of doping level on the electrochemical reduction of CO_2 on boron-doped diamond electrodes”,

Diamond & Related Material, 86 (2018) 167–172.

International Conference:

(1) J. Xu, Y. Einaga,

“Electrochemical reduction of CO_2 on sp^2 contained boron-doped diamond (BDD) electrodes”,

17th International Symposium on Electroanalytical Chemistry & 3rd International Meeting on Electrogenenerated Chemiluminescence (17th ISEAC & 3rd ECL), Changchun, China. 2019/08/24

*Excellent Poster Award was got, from top 20 of 300 presenters

Domestic Conference:

(1) J. Xu, K. Natsui, Y. Einaga,

“Electrochemical reduction of CO₂ on boron-doped diamond electrodes: boron doping level influence”,

The Electrochemical Society of Japan (ECSJ) Fall Meeting 2018, Kanazawa, Japan, 2018/09/26

(2) J. Xu, K. Natsui, S. Naoi, K. Nakata, Y. Einaga,

“Effect of doping level on the electrochemical reduction of CO₂ on boron-doped diamond electrodes”,

7th Symposium of Japan Association for Chemical Innovation/ Green & Sustainable Chemistry (JACI/GSC), Kobe, Japan, 2018/06/15

*GSC Poster Award was got, from top 25 of 300 presenters

Curriculum Vitae

Jing Xu was born in Mudanjiang, China, in 1988. She obtained the Bachelor of Science degree in Beijing University of Chemical Technology in China in 2010. With her satisfying performance during undergraduate study, she got exam-free admission opportunity for entering master program in the same university. In the year of 2012, she got the Master of Engineering degree and looking for position overseas. From 2013 to 2016, she lived in Germany and worked as a part time research assistant in the University of Siegen. From 2016, she moved to Japan and started working as a research assistant in Einaga Lab, Keio University. From the September 2017, she began her PhD course in Keio University and focused on the study of electrochemical reduction of CO₂ on BDD electrode.

Acknowledgment

This PhD thesis is finished in the memorable year of 2020. Under the pandemic spread of COVID-2019, everyone is suffering from health crisis and relevant stress. We are on the one earth, so that nations should not blame each other but fight for the virus together. With this situation, I would thank the effort of Japanese government for providing relatively stable social environment. Moreover, I would thank the embassy of China in Japan, which provide masks and medicines for Chinese oversea students including me. Without these efforts, I can not even under good healthy condition, not to mention finishing this thesis.

In the first place, I would like to express my greatest gratitude to my supervisor, Prof. Yasuaki Einaga, for your kind guidance of this work. You are the person who is leading me into the fantastic research field of BDD and encouraged me so much. By providing me fruitful academic advices during research, advanced experimental equipment, and abundant opportunities for communication inside and outside the university, my research ability has been greatly improved. Furthermore, thank you very much for your kind helps of living support, which deeply touched me and helped me so much of my life in Japan.

Likewise, I would like to thank all the members in Einaga-Lab, both staffs and students. Thank you all for discussing academic and life problems with me and helping me enjoy delighted life even in my tough period.

In addition, I would like to appreciate all the reviewer of my doctoral defense, Prof. Taku Hasobe, Prof. Yuya Oaki, and Prof. Tomoko Shimizu for all the kind questions and comments towards my work. I also thank you for the revision of this dissertation book, which makes it so much better.

Lastly, I want to thank my families. Thanks to my parents for their kind supporting both spiritual and material during my doctoral study. Especially my mother, who frequent visits Japan to help me taking care of my son so that I could concentrate on my studies. Furthermore, I want to thank my husband, Pengyu Lu, who accompanied me and helped me to optimistically face various difficulties. I am grateful to my son for letting me know that growing-up is not easy so that we should cherish the present life.

Thank you to everyone that I have met along the challenging and exciting way to PhD degree. I will continue try my best in the future work and life with your kind encourage.

Japan, July 2020

Jing Xu